HSATII RNA is induced *via* E2F3a and a non-canonical ATM-regulated DNA damage response pathway

Maciej T. Nogalski[#] and Thomas Shenk[#]

Department of Molecular Biology
Princeton University
Princeton, NJ 08544-1014, USA

[#] Corresponding authors: nogalski@princeton.edu and shenk@princeton.edu

Abstract

Recently, we documented that human cytomegalovirus (HCMV) and herpes simplex virus (HSV) infections lead to a robust induction of HSATII RNA, among other satellite repeat transcripts. HSATII RNA positively affects viral gene expression, DNA accumulation and yield, as well as has a broad influence on host cell biology. Our report also provided evidence that cooperation between at least two HCMV immediate-early proteins (IE1, IE2) is necessary for the robust induction of HSATII RNA expression. However, cellular processes contributing to the virus-induced HSATII RNA were still unknown. Here, we report that the strength with which HSATII RNA affects virus replication cycle is cell-type specific with retinal pigment epithelial cells being markedly more sensitive to levels of HSATII RNA than fibroblasts. We demonstrate that the HCMV IE1 and IE2 proteins regulate HSATII expression *via* the E2F3a transcription factor. Moreover, treatment of cells with DNA damaging agents also induced HSATII expression, and we determined that a rerouted DNA damage response (DDR) pathway, based on kinase independent ATM regulation, plays a central role in the expression of HSATII in HCMV-infected cells. Importantly, we discovered that, depending on the HSATII RNA levels, breast cancer cells showed differential sensitivity to DNA damaging drugs with enhanced cell migration seen in less metastatic cells. Additionally, we demonstrate that highly motile and proliferative phenotype of metastatic breast cancer cells can be effectively inhibited by knocking down HSATII RNA. Together, our investigation provides the molecular mechanism that links a high expression of HSATII RNA to the E2F3a-initiated induction of DDR, centered on kinase-independent functions of ATM, and to processes critical for efficient viral infection, cancer cell migration and proliferation.

Introduction

Repetitive DNA sequences comprise more than 50% of our DNA and include short (SINE) and long (LINE) interspersed nuclear elements, DNA and long terminal repeat (LTR) transposons as well as satellite repeats (1). Even though repetitive DNA elements are ubiquitous in human genome, there is a limited understanding of their functions and molecular mechanism regulating their expression. Satellite DNAs (satDNAs), which account for ~3% of the genome (1), were shown to form centromeric and pericentromeric heterochromatin, and have been implicated in chromosome organization and segregation, kinetochore formation as well as heterochromatin regulation (2). With improvements in the next-generation sequencing (NGS), these genomic sites, previously thought to be largely transcriptionally inert, were showed to produce non-coding RNAs (ncRNAs), which contribute to the role of satDNAs in chromosome and heterochromatin functions (3-5).

Importantly, altered patterns of transcription, including a deregulation of ncRNAs, often occur in tumors (6-8). Many ncRNAs were found in cancer cells originating from satDNA regions of the genome, such as human alpha-satellite repeat (Alpha/ALR), human satellite II (HSATII) and its mouse counterpart GSATII (9-11). HSATII and GSATII have a distinct nucleotide motif usage from that commonly seen in most non-coding transcripts, resulting in their immunostimulatory potential (12). Notably, transcriptomic signatures in cancers were reported to closely resemble those gene expression profiles characteristic to anti-viral responses (13, 14). Additionally, high expression of Alpha/ALR and HSATII RNAs was suggested to lead to their reverse transcription and stable reintegration into the human genome, expanding their genomic copy numbers (15). Importantly, elevated copies of genomic HSATII were found to be common in primary human colon tumors and correlated with lower survival rates of colon cancer patients (15), stressing the importance of investigating molecular mechanisms regulating the satellite repeat expression.

While some satellite repeat transcription was found to be stress-dependent (16) or triggered during apoptotic, differentiation or senescence programs in cells (17, 18), HSATII transcription was reported to be refractory to these generalized environmental stressors and was induced when cancer cells were grown only in non-adherent conditions or as xenografts in mice (15). Therefore, there was an unfulfilled need for the development of additional, well-controlled biological systems, allowing expedited interrogation of the mechanisms responsible for the satellite repeat expression and functions.

It is estimated that 12% of all cancers have a viral etiology and often are linked to persistent or chronic infections (19). Viruses are known to have a broad effect on cells, regulating many biological processes often in a similar matter to those seen in cancer cells. Those biological changes caused by infections do not only resemble cancer, but might in some cases lead to oncogenesis (20). As high expression of satellite repeats was strongly associated with several cancers (3, 9, 11, 21), our research aimed to

102 evaluate a possibility of viral infection as an inducer of this phenomenon.
103 Knowing that the broad spectrum of biological changes seen in human cytomegalovirus (HCMV)-
104 infected cells resemble those common to cancers, including an activation of pro-oncogenic pathways,
105 changes in cellular metabolism and increased cell survival (22-27), we used HCMV as a model system.
106 HCMV is a β-herpesvirus that infects a large percentage of the adult population worldwide. Infection in
107 immunocompetent people is typically asymptomatic. In contrast, HCMV is a leading opportunistic
108 pathogen in immunosuppressed individuals (28-30), and a major infectious cause of birth defects (31).
109 HCMV causes chronic diseases and a hallmark of severe HCMV infection is the involvement of multiple
110 organs (32). HCMV has been also suggested to play a role, perhaps an oncomodulatory role, in the
111 etiology of several human cancers (24, 33-39). However, its high prevalence has made it difficult to
112 prove causality in the disease (40).
113 Recently, we determined that HCMV infection induces HSATII RNA, among other satellite repeat
114 transcripts, to the same extent as reported for tumor cells (41). By knocking down HSATII RNA in
115 HCMV-infected cells, we showed that this satellite repeat transcript positively affects viral gene
116 expression, DNA accumulation and yield (41). Moreover, our study suggested that HSATII RNA
117 influences several cellular processes, such as protein stability, posttranslational modifications and
118 particularly the high levels of HSATII RNA lead to the increased motility of infected cells (41).
119 Therefore, it is conceivable that satellite repeat transcripts could enhance the fitness of both the virus
120 and cancer cells in the environment of the host by regulating the same molecular pathways. Our report
121 also provided evidence that cooperation between at least two HCMV immediate early proteins (IE1,
122 IE2) is necessary for the robust induction of HSATII RNA expression (41). Additionally, high levels of
123 HSATII were found *in vivo* in CMV colitis, indicating that satellite repeat transcripts could provide
124 another regulatory layer to the processes important in pathology of diseases also associated with
125 herpesviruses, such as colitis, retinitis, encephalitis, pneumonia, hepatitis and cancer (42, 43).
126 Therefore, our studies not only determined that HSATII RNA has broad effects on viral and cellular
127 biology, but also viral infection can be used effectively for a controlled induction of satellite repeat
128 RNAs, paving a path to extend our investigations into the molecular mechanisms governing satellite
129 repeat expression.
130 Interestingly, HCMV IE1 and IE2 proteins are known to regulate Rb and E2F protein families, leading to
131 efficient viral replication through the induction of DNA damage response (DDR) (44, 45). The family of
132 E2F transcription factors consists of nine members. Specifically, E2F1-E2f3a are considered strong
133 transcriptional activators and E2F3b-E2F8 function as transcriptional repressors (46, 47). E2F1-E2F3
134 are regulated by the retinoblastoma tumor suppressor protein (Rb) and the activities of E2F4-E2F5 are
135 govern by two other members of Rb family, p107 and p130 (48). Upon phosphorylation Rb, p107 or
136 p130 are inactivated and dissociate from E2Fs, allowing E2Fs to affect transcription of their target

genes (49, 50). Importantly, E2Fs were showed to bind promoters of genes involved in the DNA damage checkpoint and repair pathways as well as chromatin regulation (51).

Recently, Alpha/ALR RNA has been found in breast cancer cells to associate with breast cancer type 1 susceptibility protein 1 (BRCA1) and was implicated in tumor formation in mice (52).

Breast cancers are a leading cause of cancer-related mortality in women (53). Triple-negative breast cancers (TNBCs), which lack the expression of estrogen receptor, progesterone receptor and human epithelial growth factor receptor, are non-responsive to hormonal therapies, more difficult to treat and considerably more aggressive (54).

Deregulated DDR pathways and cell cycle checkpoints allow cancer cells to achieve high proliferation rates, but at the same time make them more susceptible to DNA damaging agents; a characteristic central to their use as anticancer drugs (55, 56). However, with the widespread use of DNA damage therapies and their clinical successes, these therapies are known to be toxic to non-cancer cells, often lead to drug resistance (55, 56) and rise concerns about a development of *de novo* primary tumors (57).

Based on their mechanism of action and type of induced damage, DNA damaging agents can activate specific DNA damage repair pathways, such as the nucleotide excision repair pathway (NER), the base excision repair pathway (BER), and two pathways targeting DNA double-strand breaks (DSBs): homology directed repair (HDR) and non-homologous end joining (NHEJ). Importantly, there is a considerable crossover between these pathways with the use of DDR regulatory molecules, including the Ataxia-telangiectasia mutated (ATM), ATM and Rad3 related (ATR) and the DNA-dependent protein kinase catalytic subunit (DNA-PKcs) (58). The activation of these three DDR regulatory molecules leads to phosphorylation of histone variant H2AX at serine 129, named γ-H2AX, which is believed to be principal in DNA repair processes and is often considered as a sensitive marker for DNA DSBs (59). The activation of ATM and ATR leads to activation of two downstream kinases, checkpoint 1 and 2 (Chk1 and Chk2), which ultimately regulate the p53 activity in a context dependent manner (60-62).

Additionally, there is also a growing appreciation of the role that ncRNAs play in DDR, as long ncRNAs (lncRNAs) and microRNAs were found induced upon DNA damage and to regulate DDR (63).

Among chemical compounds that activate DDR, treatments with etoposide or lead to DSBs. Etoposide, similarly to doxorubicin, is an anticancer agent working through poisoning topoisomerase II, stabilizing DNA-protein complexes, which ultimately leads to stalled replication forks (64). Zeocin belongs to a bleomycin/phleomycin-family of antibiotics and as a radiomimetic has similar effects on DNA as ionizing radiation (IR) (56), and has been suggested as a chemotherapy candidate (65). Interestingly, etoposide and IR were documented to induce a transcription and retrotransposition of SINEs (66, 67). Based on these data, we speculated that the expression of human satellite repeats could be regulated through the induction of DDR.

172 Intriguingly, our newest results presented here describe that the strength with which HSATII RNA
173 affects viral processes in infected cells is cell-type specific, as in epithelial cells a much stronger
174 influence of HSATII RNA was seen on several aspects of viral replication when compared to its effects
175 in infected human fibroblasts. Importantly, we uncovered that HSATII induction is specifically regulated
176 by E2F3a isoform and involves a unique ATM-based, but p53-independent, DDR response pathway.
177 Moreover, our data provided evidence for a role of HSATII RNA in exasperating the aggressive
178 phenotype of breast cancer cells, localizing the newly described molecular mechanism of HSATII
179 induction as an important target for future antiviral and anticancer treatments.
180
181
182 **Results**
183
184 **HSATII KD has strong effect on HCMV infection in epithelial cells.** Our previous report described
185 the induction of satellite repeat expression in cells infected by herpesviruses and demonstrated that at
186 least one satellite RNA, HSATII RNA, positively affects viral gene expression, vDNA accumulation and
187 ultimately HCMV yield using human foreskin fibroblasts (HFFs) as an infection model system (41). Our
188 highly efficient and specific method of knocking down HSATII RNA produced a strong effect on viral
189 gene expression, however reduced the accumulation of vDNA by ~20% and viral infectious progeny by
190 a factor of ~8 when compared to control infected fibroblasts (41). Interestingly, our investigation
191 determined that kinetics of HSATII expression are accelerated and IE1/IE2-expression leads to
192 stronger higher levels of HSATII RNA in retinal pigment epithelial (ARPE-19) cells when compared to
193 HFFs (41). Intrigued by this fact and knowing that even though HCMV replication is most often studied
194 in fibroblasts, the virus infects a range of cell types, causing often biologically unique cellular changes
195 and underlining their specific roles in HCMV pathogenesis (68). The retinal pigment epithelium is the
196 primary site of HCMV infection in the eye and CMV retinitis is the most common CMV disease in
197 immunocompromised patients (69, 70). Therefore, we decided to analyze the effect of HSATII RNA on
198 viral infection in epithelial cells that support HCMV productive infection and were critical in establishing
199 the viral pentameric glycoprotein complex as essential for infection of epithelial, endothelial and myeloid
200 cells (71-77).
201 Similarly to results obtained using HFFs (41), ARPE-19 cells transfected with two individual HSATII-
202 LNAs (HSATII-LNA #1 or HSATII-LNA #2) or with their combination efficiently decreased HSATII
203 transcript levels by 78-86% or 96%, respectively, when compared to cells transfected with control LNA
204 (NT-LNA) (Figure 1A). To assess the effect of HSTAII RNA on HCMV infection in ARPE-19 cells, we
205 first monitored viral protein levels up to 96 hours post infection (hpi) with the epithelial cell-grown HCMV
206 strain TB40/E (TB40/E-GFP-epi). Cells were transfected with NT-LNA or with both HSATII-LNAs 24 h

207 before HCMV infection at 1 $TCID_{50}$/cell and protein levels were analyzed using the western blot assay.
208 HSATII RNA did not affect IE1 protein levels up to 72 hpi, however, HSATII knockdown (KD) severely
209 decreased IE1 protein at 96 hpi (Figure 1B), which differs from kinetics of IE1 expression seen in
210 infected fibroblasts lacking HSATII RNA (41). Additionally, IE2 and the early and late viral proteins
211 accumulated to much lower levels in HSATII KD cells compared to control cells at each time tested
212 (Figure 1B). Consistent with perturbed viral protein expression, HSATII KD strongly reduced the level of
213 intracellular vDNA at 72 (~24x lower) and 96 (~5x lower) hpi compared to its levels in infected cells with
214 normal, high levels of HSATII RNA (Figure 1C). HSATII KD reduced the accumulation of infectious
215 virus at 96 and 120 hpi by a factor of ~1750 or ~800, respectively, when compared to viral yield from
216 NT-LNA-treated control cells as evaluated by the TCID50 assay (Figure 1D). Strikingly, the effect of
217 HSATII KD seen in ARPE-19 cells is ~150x stronger than what we observed in HFFs (41). To further
218 assess the effect of HSATII on virus production in ARPE-19 cells, we monitored the accumulation of
219 intracellular and extracellular virus at 96 hpi calculating plaque forming units (PFUs). In HSATII KD
220 cells, infectious virus was reduced inside infected cells by a factor of ~160 and the amount of virus
221 released from cells was decreased by a factor of ~100 when compared virus levels in media collected
222 from NT-LNA-treated cells (Figure 1E). These data demonstrate that HSATII RNA has at least 12-20x
223 more potent effect on viral progeny production in ARPE-19 cells as compared in HFFs. Observing that
224 ARPE-19 cells respond more robustly to fluctuations in HSATII RNA levels, we chose to use ARPE-19
225 cells in our investigations focused on identifying molecular mechanism(s) responsible for HSATII
226 induction.
227
228 **DNA damage response regulates HSATII expression.** The data showed so far in this report, together
229 with our previously published results (41), depict HSATII RNA as an important regulatory factor not only
230 in processes associated with viral infection but also affecting several cellular processes, such as protein
231 stability, posttranslational modifications, and cellular movement. Additionally, high expression of certain
232 satellite repeat transcripts correlated with lower survival rates of colon cancer patients (15) and were
233 suggested to affect the epigenetic regulation in cancer cells (11). Therefore, it is conceivable that
234 satellite repeat transcripts could enhance the fitness of both the virus and cancer cells, suggesting that
235 in both diseases a similar molecular mechanisms could be used for their induction. Our recent report
236 provided evidence that cooperation between at least two viral immediate early proteins (IE1, IE2) is
237 necessary for the robust induction of HSATII RNA expression (41). As HCMV IE1 and IE2 proteins are
238 known to regulate Rb and E2F protein families, affecting DDR induction and leading to efficient viral
239 replication (44, 45), we speculated that DDR could play a role in the expression of human satellite
240 repeats.
241 Initially, to test this hypothesis, ARPE-19 cells were stressed by UV-C irradiation, H_2O_2 treatment or

242 serum withdrawal as all these treatment lead to DDR activation (78-80). Based on RT-qPCR, the
243 exposure of ARPE-19 cells, which normally express HSATII RNAs at very low basal levels, to UV-C
244 energy, H_2O_2 or serum withdrawal did not result in a strong HSATII induction (Figure 2A), as seen in
245 virus-infected cells (100-1000x higher) (41). As a control for efficient DDR activation and induction of
246 p53 activity, the expression levels of p53-dependent cyclin-dependent kinase inhibitor 1 (p21; encoded
247 by CDKN1A gene) (78) and p53-regulating Damage Induced Noncoding (DINO) lncRNA (81) were
248 monitored. As expected, both were elevated in cells exposed to UV-C irradiation, H_2O_2 treatment or
249 serum withdrawal (Figure 2A).
250 While UV-C irradiation is believed to cause DNA double-strand brakes (DSBs), the specific role of UV-
251 C in DNA damage depends on the replicative state of treated cells, as those breaks usually arise from
252 the replication of unrepaired UV-induced DNA lesions (82, 83). Therefore, it was possible that UV-C
253 treatment was either not efficient in inducing HSATII RNA or that the specific DNA damage induced
254 was not responsible for satellite repeat expression. As the creation of DNA DSBs was suggested to be
255 important to induce an expression of SINEs (66, 67), we next tested the effects of two DNA damaging
256 agents, zeocin and etoposide. Both drugs are known to induce DNA DSBs (84, 85) and, in the case of
257 etoposide, stimulated the expression of mouse B2 SINE RNA (66, 67). ARPE-29 cells were exposed to
258 increasing concentrations of zeocin or etoposide and HSATII, CDKN1A and DINO expression was
259 monitored. Zeocin caused rapid induction of HSATII transcription (~100x) starting at 25 μg/mL and
260 HSATII RNA levels increase in a dose-dependent manner reaching ~500x increase at the zeocin
261 concentration of 400 μg/mL when compared to HSATII RNA levels in control cells (Figure 2B).
262 Etoposide treatment also resulted in elevated HSATII RNA levels starting to be detected at 25 μM
263 (~50x increase), further increasing with a rising concentration of etoposide and being ~700x higher in
264 cells exposed to 500 μM of etoposide than HSATII RNA levels in control cells (Figure 2C). CDKN1A
265 and DINO expression closely trailed dynamics of HSATII RNA reaching 6-7-fold induction in cells
266 exposed to 400 μg/mL of zeocin (Figure 2B) and ~25-fold induction in cells treated with 500 μM of
267 etoposide (Figure 2C). Importantly, no ARPE-19 cell toxicity was detected at any concentrations of the
268 drugs tested at 24 hpt (Figure 2B and 2C). For our further studies, we decided to use 200 μg/mL of
269 zeocin and 200 μM of etoposide as both concentrations showed to elevate HSATII RNA to levels seen
270 in cells infected with HCMV at 3 TCID50/cell, therefore giving a good experimental conditions to
271 compare HCMV- and DNA damaging drug-based induction of HSATII RNA.
272 Upon exposing ARPE-19 cells to 200 μg/mL of zeocin or 200 μM of etoposide, we monitored kinetics of
273 HSATII, CDKN1A and DINO expression by RT-qPCR from 0 to 24 hours post treatment (hpt). Our
274 analysis demonstrated that HSATII expression starts to increase approximately 12 h upon the initial
275 treatment with either zeocin or etoposide, reaching levels equal to 300-fold induction at 24 hpt

276 compared to solvent control-treated cells (Figure 2D and 2E). Dynamics of CDKN1A and DINO
277 expression are accelerated compared to HSATII expression, as both transcripts reached their
278 maximum levels within the first 2-4 hpt (Figure 2D and 2E), suggesting a possible decoupling of
279 DDR/p53-dependent pathways from the mechanism regulating HSATII induction.
280 To compare effect of HCMV and zeocin on HSATII induction, ARPE-19 cells were mock- or HCMV
281 (TB40/E-GFP-epi)-infected at 1 $TCID_{50}$/cell, or treated with 100 μg/mL of zeocin or H_2O as a solvent
282 control. Of note, the concentration of zeocin was adjusted to match levels of HSATII expression in cells
283 infected with HCMV at 1 $TCID_{50}$/cell. After 24 h, RNA samples were collected, RNA was isolated and
284 analyzed using RNA-seq. RNA-seq reads were quality filtered and mapped to human genome
285 assembly hg19 using the STAR aligner (86). Read coverage tracks at the HSATII-rich locus on
286 chromosome 16 were visualized by the Integrative Genomics Viewer (IGV) using STAR-created BAM
287 files. The data from mock-infected cells and untreated cells showed almost no reads mapped to this
288 HSATII locus (Figure 2F). However, this HSATII–rich locus spanning approximately 17 kb of DNA was
289 richly covered by HSATII-specific reads and the read coverage tracks showed a similar distribution of
290 read coverage peaks based on the RNA-seq data from HCMV-infected or zeocin-treated ARPE-19 cells
291 (Figure 2F). Therefore, these data strengthened our notion about common mechanisms responsible for
292 HSATII expression in both HCMV-infected and DNA damaging drug-treated cells and about possibilities
293 to identify them using these methods of inducing the expression of satellite repeat transcripts.
294
295 **Zeocin partially mimics transcriptional effect of HCMV in treated cells.** To assess common
296 biological processes regulated in infected cells and cells with chemically damaged DNA, ARPE-19 cells
297 were mock- or HCMV (TB40/E-GFP-epi)-infected at 1 $TCID_{50}$/cell, or treated with 100 μg/mL of zeocin
298 or H_2O as a solvent control. The RNA-seq analysis determined that 567 cellular genes were
299 significantly ($q < 0.05$) expressed in HCMV-infected and 827 genes in zeocin-treated cells (Figure 3A).
300 Additionally, our analysis discovered that the same 87 differentially expressed genes were regulated in
301 both HCMV-infected and zeocin-treated cells (Figure 3A). Those genes upon our further analysis based
302 on the Gene Set Enrichment Analysis (GSEA) (87) using the hallmark gene set of the Molecular
303 Signatures Database (MSigDB) (88) were strongly associated with gene subsets related to E2F targets,
304 cell cycle checkpoints, epithelial-to-mesenchymal transition, interferon response, mTOR1 and
305 hedgehog signaling pathways, DNA repair and apoptosis (Figure 3B). As we were interested in
306 determining the common molecular mechanisms that govern HSATII induction in infected and zeocin-
307 treated cells, we focused our attention on the most significantly enriched process associated with the
308 family of E2F transcription factors.
309
310 **Transcription factor E2F3a regulates HSATII expression.** Knowing that the Rb proteins are

311 regulated during HCMV infection (89-91), we decided to screen Rb-regulated E2F1-E2F5 for their role
312 in the HSATII expression. ARPE-19 cells were transfected with control siRNA (NT siRNA) or specific
313 siRNAs targeting E2F1, E2F2, E2F3, E2F4 or E2F5. 24 h later, the cells were infected with HCMV
314 (TB40/E-GFP-epi) at 1 $TCID_{50}$/cell. RT-qPCR assay performed on total RNA collected at 24 hpi
315 uncovered that all specific siRNAs efficiently downregulated their target transcripts (E2F1 by 86%;
316 E2F2 by 91%, E2F3a by 79%, E2F3b by 75%; E2F4 by 66% and E2F5 by 83%) compared to their
317 expression in control cells (Figure 4A). However, only E2F3 KD led to a strong (84%) decrease of
318 HSATII RNA (Figure 4A). Of note, E2F3 siRNA used in our studies decreased expression of both E2F3
319 isoforms. The E2F3 locus encodes two isoforms, E2F3a and E2F3b (92, 93), which are generated from
320 two separate promoters (94). E2F3a and E2F3b were reported to have often overlapping but also
321 different effects on biological processes (95-98). Classically, E2F3a is considered a transcriptional
322 activator and E2F3b is a transcriptional repressor (46, 47).
323 Our previous report documented that two HCMV proteins IE1 and IE2 cooperate to induce HSATII
324 expression (41), thus we were intrigued by a possibility of IE1 and IE2 regulating HSATII induction
325 through E2F3a/b. To investigate this idea, we used ARPE-19 cells containing tetracycline-inducible
326 system for the expression of HCMV IE1 and IE2 proteins (41). These cells were transfected with E2F3
327 siRNA 24 h before cells were infected with HCMV (TB40/E-GFP-epi) at 1 $TCID_{50}$/cell. Again E2F3
328 siRNA-treated cells showed an efficient E2F3a and E2F3b KD (by 84% and 87%, respectively)
329 compared to NT siRNA-transfected cells (Figure 4B). Importantly, E2F3a/b KD led to a substantial
330 decrease (by 85%) of HSATII RNA at 48 h post the doxycycline treatment as compared to its levels in
331 IE1/IE2-expressing cells transfected with control siRNA (Figure 4B).
332 To distinguish if one of E2F3 isoforms is more important in regulating HSATII expression, we decided to
333 overexpress E2F3a and E2F3b isoforms separately. ARPE-19 cells were transfected either with
334 plasmids expressing E2F3a or E2F3b (pCMV-Neo-Bam E2F3a or pCMV-Neo-Bam E2F3b (99),
335 respectively), E2F1 or E2F2 (pCMVHA E2F1 or pCMVHA E2F2 (100), respectively) or control plasmid
336 pCMV-Neo-Bam (101). 72 h post transfection, RNA samples were collected. Our RT-qPCR analysis
337 uncovered that only cells expressing E2F3a showed a significant (~12-fold) increase in HSATII RNA
338 and, notably, the expression of E2F3b isoform had even a counteracting effect on HSATII expression
339 (Figure 4C). Additionally, the elevated expression of E2F1 and E2F2 did not result in the HSATII
340 induction (Figure 4C), which support our results suggesting among E2Fs a sole involvement of E2F3 in
341 HSATII induction (Figure 4A and 4B).
342 As elevated expression of E2F3a led to increase levels of HSATII in our experiments, there was a
343 possibility that this transcription factor is also elevated in HCMV-infected cells and/or cells treated with
344 DNA damaging agents. To evaluate this idea, we tested E2F3a expression at 24 h post HCMV infection
345 or treatments with either zeocin or etoposide. Our analysis determined that, even though with different

346 intensities, exposures to the virus or DNA damaging drugs resulted with a significant increase of E2F3a
347 expression (Figure 4D).
348 Interestingly, our western blot analysis of E2F3a protein levels in HCMV-infected and IE1/IE2-
349 expressing cells discovered that E2F3a isoform became elevated in HCMV-infected cells only at 72 and
350 96 hpi (Figure 4E). On the other hand, IE1/IE2-expressing cells were characterized by a strong
351 expression of E2F3a even at 24 h post doxycycline treatment (Figure 4E). Being aware that IE1/IE2-
352 expressing cells have slower dynamics of HSATII expression compared to its expression in HCMV-
353 infected cells (41), we speculate that E2F3a is not solely responsible for HSATII induction and other
354 unidentified transcription factors might be also involved in the high expression of HSATII seen in
355 HCMV-infected and DNA damaging drug-treated cells.
356 Our data strongly support HSATII RNA as an important regulator of viral gene expression [Figure 1 and
357 (41)]. As we established the importance of E2F3a isoform in HSATII expression, we wondered what
358 effect E2F3 has on viral gene expression. Therefore, we transfected ARPE-19 cells with control siRNA
359 or E2F3 siRNA 24 h before HCMV infection. RNA samples were collected at 48 hpi and viral gene
360 expression was assessed by monitoring levels of UL123, UL37x1, UL26, UL54, UL 82 and UL99 viral
361 transcripts. Our analysis determined that except UL123, which mirrored the effect of HSATII RNA on
362 viral proteins (Figure 1B), all tested viral transcripts were negatively affected in E2F3 KD cells when
363 compared to control cells (Figure 4F).
364 As E2F3a emerged from our investigation as an important regulator of HSATII expression in both
365 HCMV-infected and DNA damaging drug-treated cells, we were curious if the activation of DDR may
366 provide an advantage for HCMV infection. We treated ARPE-19 cells with 200 μg/mL of zeocin and 24
367 h later the cells were infected with HCMV. Media from control cells and zeocin-pretreated cells was
368 collected at 96 hpi to assess virus yield. Results obtained from the TCID50 assay showed that Zeocin-
369 pretreated cells produced in average 6x more infectious progeny than control cells (Figure 4G),
370 demonstrating a favorable environment for viral infection in cells with the activated DNA DSB-based
371 DDR. Therefore, it became even more important to determine what aspects of DDR lead to HSATII
372 expression and ultimately efficient viral replication.
373
374 **ATM-based DNA damage response regulates HSATII expression.** As the Rb/E2F regulation is
375 advantageously utilized during HCMV infection (44, 45, 89-91) and the transcriptional activity of E2Fs is
376 know to regulate DDR (102-104), we focused our attention on identifying DDR pathway(s) involved in
377 HSATII expression. The type of DNA damage governs the activation of specific DDR pathways
378 involving ATM, ATR and/or DNA-PK (58, 60, 105) and the establishment of γ-H2AX is considered as a
379 sensitive marker for DNA DSBs (59).

380 Initially, we tested the ability of HCMV or zeocin to induce γ-H2AX. ARPE-19 cells were left untreated,
381 HCMV (TB49/E-GFP-epi)-infected at 1 $TCID_{50}$/cell, or treated with 100 μg/mL of zeocin for 24 hours.
382 Cells were fixed, stained with antibodies recognizing γ-H2AX proteins, nuclei were counerstained with
383 the Hoechst stain and representative microscopy pictures were taken. The immunofluorescence-based
384 assay showed that both HCMV-infected and zeocin-treated cells had elevated signal for γ-H2AX,
385 however, cells exposed to zeocin were characterized by a much higher number of γ-H2AX-positive cells
386 (65%) than HCMV-infected cells (14%) (Figure 5A and 5B).
387 Knowing that both HCMV and trigger the accumulation of γ-H2AX in treated cells, we decided to
388 scrutinize possible contributions of ATM, ATR and/or DNA-PK in the induction of HSATII RNA. ARPE-
389 19 cells were transfected with NT siRNA or specific siRNAs targeting ATM, ATR or PRKDC transcripts.
390 24 h later, the cells were infected with HCMV (TB40/E-GFP-epi) at 1 $TCID_{50}$/cell, or treated with 100
391 μg/mL of zeocin for 24 h. All specific siRNAs produced strong (75-90% decrease) downregulation of
392 targeted transcripts (Figure 5C and 5D). However, only ATM siRNA treatment led to a significant
393 decrease of HSATII RNA levels (~70% decrease) either in HCMV-infected or zeocin-treated cells
394 (Figure 5C and 5D).
395 To confirm the ATM involvement in HSATII expression uncovered by our siRNA-based screen, we used
396 ataxia-telangiectasia [A-T (-)] fibroblasts that possess a functionally mutated ATM gene as well as a
397 derivative of this cell line, A-T (+) cells with a stably expressed functional ATM [A-T (+)] (106, 107).
398 Cells were either mock- or HCMV (TB40/E-GFP)-infected at 1 $TCID_{50}$/cell, exposed to solvent controls,
399 H2O or DMSO, or treated with 100 μg/mL of zeocin or 100 μM of etoposide for 24 h. Infected or DNA
400 damaging drug-treated A-T (+) cells were characterized by a strong induction of HSATII RNA
401 (increased by 71x, 137x and 6x in HCMV-, zeocin- and etoposide-treated cells, respectively) and,
402 except HCMV-infected cells, treatments also led to the higher expression of CDKN1A and DINO, again
403 suggesting lack of p53-dependent regulation in HSATII induction (Figure 5E). A-T (-) cells had about 6-
404 fold lower expression of HSATII upon HCMV infection or treatments with DNA damaging drugs when
405 compared to its expression in A-T (+) cells (Figure 5E). Moreover, zeocin and etoposide treatments, but
406 not HCMV infection, of A-T (-) cells resulted in significantly lower expression levels of CDKN1A and
407 DINO (~15x and ~6x lower, respectively) when compared to their expression in A-T (+) cells (Figure
408 5E). Together these data strongly indicate that among DDR regulatory factors ATM solely plays an
409 important role in HSATII expression.
410 A-T (-) cells possess a missense mutation in the carboxy-terminal PI 3-kinase-like domain that leads to
411 very low levels of mutated ATM protein (107). As ATM mostly exercises its function through its kinase
412 activity (60-62), we intended to directly assess the importance of ATM kinase activity in HSATII
413 induction using Ku-55933 or AZ31 [two specific ATM kinase inhibitors (108, 109)]. Ku-55933 and AZ31

414 did not show any strong effect on viability of treated cells when tested at concentrations up to 50 μM
415 using a 3-(4,5-dimethylthiazol-2-yl)-5-(3-carboxymethoxyphenyl)-2-(4-sulfophenyl)-2H-tetrazolium
416 (MTS)-based CellTiter 96 AQueous One Solution Cell Proliferation Assay (Figure 5G). However,
417 because we noticed some morphological changes in treated cells at the highest (50 μM) concentration,
418 we decided to use Ku-55933 and AZ31 at the concentration of 20 μM, which is in a range of
419 concentrations these drugs have been used by others (108-110).
420 ARPE-19 cells were treated for 2 h with either Ku-55933 or AZ31 at the concentration of 20 μM or
421 DMSO as a solvent control. Next, cells were treated with zeocin at the concentration of 100 μg/mL.
422 Remarkably, we determined that at 24 hpt neither Ku-55933 nor AZ31 inhibitors affected HSATII RNA
423 levels (Figure 5F). However, as suspected in case of an effective inhibition of ATM kinase activity, both
424 treatments negatively (~70% decrease) affected expression of CDKN1A and DINO transcripts when
425 compared to DMSO-treated control cells (Figure 5F). Based on our results, we suggest that HSATII
426 expression is regulated via ATM but independently from its kinase activity.
427
428 **HSATII expression is induced *via* Chk1/2- and p53-independent pathway**. To evaluate our
429 hypothesis about ATM kinase-independent induction of HSATII, we focused on the ATM downstream
430 signaling events. ATM and ATR together with Chk1 and Chk2, encoded respectively by CHEK1 and
431 CHEK2 genes, create evolutionary conserved ATM-Chk2 and ATR-Chk1 signaling cascades regulating
432 the p53 activity in a context dependent manner (60-62).
433 Based on our data, we hypothesized that among the two protein kinase cascades the ATM-Chk2 had
434 the highest possibility of being involved in HSATII induction. To test this idea, we utilized siRNA-based
435 knockdown of CHEK1 and CHEK2 transcripts. 24 hours prior HCMV (TB40/E-GFP-epi)-infection at 1
436 $TCID_{50}$/cell or the treatment of zeocin at the concentration of 100 μg/mL, ARPE-19 cells were
437 transfected with NT siRNA or siRNA specifically targeting CHEK1 and CHEK2 transcripts, resulting in a
438 robust (98% and 75%, respectively) decrease of these transcripts at 24 hpi/hpt (Figure 6A). However,
439 we did not detect any statistically significant effect of CHEK1 or CHEK2 KDs on HSATII induction
440 neither in HCMV-infected nor zeocin-treated cells when compared to their expression in control cells
441 (Figure 6A), suggesting that the canonical ATM-Chk2-dependent signaling does not play an important
442 role in the expression of HSATII.
443 Intrigued by these results, we decided to investigate also the involvement of p53 in HSATII induction.
444 Initially ARPE-19 cells were infected with HCMV (TB40/E-GFP-epi) at 1 $TCID_{50}$/cell or treated with 100
445 μg/mL of zeocin and CDKN1A and DINO expression were monitored at 24 and 120 hpi/hpt to assess
446 activity of p53. Corresponding to our results obtained from ataxia telangiectesia cells (Figure 5E),
447 HCMV infection did not affect levels of the p53-regulated CDKN1A (p21) and DINO lncRNA at 24 hpi

448 (Figure 6B). However, their levels increased in HCMV-infected cells at 120 hpi (Figure 6C), supporting
449 previously reported effect of HCMV IE proteins on p21 activity (111-113). Of note, a decrease of p21
450 protein level was also observed in HCMV-infected cells, a discrepancy that might be related to the use
451 of different experimental designs, cell types and/or culture conditions (114). On the other hand, cells
452 treated with zeocin were characterized by elevated expression of CDKN1A and DINO at both tested
453 time points (Figure 6B and 6C). Importantly, all those treatments led to dramatic (200-500x) increase in
454 HSATII RNA at 24 and 120 hpi/hpt when compared to untreated cells (Figure 6B and 6C).
455 Next, control and p53 KD ARPE-19 cells were HCMV (TB40/E-GFP-epi)-infected or treated with 100
456 μg/mL of zeocin and again HSATII, CDKN1A and DINO expression were assessed at 24 and 120
457 hpi/hpt. TP53 siRNA strongly (by ~83% and 87%) decreased targeted transcript at both times tested
458 when compared to TP53 expression in NT siRNA-treated cells (Figure 6D and 6E). Importantly, TP53
459 siRNA had very limited effect (10% decrease) on HSATII expression and it was only seen at 120 hpi
460 when compared to control cells (Figure 6E). All other experimental condition tested either did not have
461 any effect or slightly increased HSATII expression, as it was seen in zeocin-treated cells at 120 hpt
462 (Figure 6E).
463 Interestingly, p53 KD did not influence CDKN1A and DINO expression at 24 h post HCMV infection
464 (Figure 6D), but significantly (~65%) decreased both transcripts at 120 hpi. In comparison, p53 KD
465 strongly (80% decreased) affected CDKN1A and DINO expression at both 24 and 120 h post zeocin
466 treatment (Figure 6E). Together, our results strongly support a notion of p53- and canonical ATM
467 kinase-independent regulation of HSATII expression.
468
469 **DNA damage-induced HSATII RNA enhances motility and proliferation of breast cancer cells.**
470 Due to the high expression of E2Fs in breast cancers, recently these transcription factors have been
471 suggested as promising biomarkers and therapeutic targets for breast cancers treatments (115).
472 Additionally, ATM mutations that cause in biallelic individuals ataxia-telangiectasia were found to
473 present a higher risk of developing breast cancer in ATM heterozygotes (116, 117). As our results
474 indicated that HSATII induction is regulated via the ATM kinase-independent mechanism, a high
475 HSATII expression was detected in several cancers, including breast cancer (9, 11) and a positive
476 correlation between HSATII expression and cancer patients survival was documented (15), we wanted
477 to assess HSATII expression levels and the effect of DDR-inducing drugs on breast cancer cell lines
478 characterized by varying degree of p53 status, hormonal dependency and tumor aggressiveness. We
479 tested less invasive: MDA-MB-175VII (ER+, PR-, HER2-, p53 wt), MDA-MB-361 (ER+, PR+/-, HER2-,
480 p53 wt), MCF7 (ER+, PR+, HER2-, p53 wt), more metastatic triple negative breast cancer (TNBC) cell
481 lines with mutated p53: SUM1315M02, MDA-MB-231, BT-549 in comparison with MCF-10A, a breast
482 epithelial cells, and ARPE-19 cells (118). Cells were cultured to allow adherence using identical media

483 conditions to prevent variations in results potentially caused by different culture conditions. Upon
484 reaching 80-90% confluency, RNA samples were collected. Our RT-qPCR-based assay determined
485 that the basal levels of HSATII RNA in MCF-10A, MCF-7, MDA-MB-175VII and MDA-MB-361 were 5-
486 6x higher when compared to HSATII expression in ARPE-19 cells (Figure 7A). Importantly, our assay
487 found that SUM1315M02, MDA-MB-231, BT-549 were characterized with higher levels of HSATII RNA
488 compared to less invasive breast cancer cells or ARPE-19 cells (Figure 7A).
489 Seeing these results, we decided to test a response of MCF-7, MCF-10A, MDA-MB-361 and
490 SUM1315MO2 cells to the zeocin treatment assaying for HSATII RNA. Cells were treated with 200
491 μg/mL of zeocin and HSATII expression was assessed at 24 and 96 hpt. All tested cells responded to
492 zeocin by elevating levels of HSATII RNA compared to its levels in solvent control-treated cells (Figure
493 7B). Additionally, the longer exposure (96 h) of cells to the DNA damaging drug correlated with an even
494 higher expression of HSATII (Figure 7B).
495 In our previous report, high HSATII RNA levels were showed to positively affect motility of HCMV-
496 infected ARPE-19 cells (41) and our RNA-seq analysis also determined that genes commonly regulated
497 by HCMV and zeocin associated with EPITHELIAL_MESENCHYMAL_TRANSITION gene set (Figure
498 3B). As we uncovered that DNA damaging drugs led to the high HSATII expression in treated cells, we
499 wondered if zeocin treatment might influence migratory characteristics of exposed cells. To test this
500 idea, ARPE-19, MCF-7 and SUM1315MO2 cells were treated with 200 μg/mL of zeocin or DMSO as a
501 solvent control for 24 h. Next, the transwell migration assay (119) was performed using equal numbers
502 of cells and cell motility was assessed 24 h later. Our analysis uncovered that both ARPE-19 and MCF-
503 7 cells showed an increased (~ 70% and 100% increase, respectively) migratory phenotype upon
504 zeocin treatment when compared to solvent control-treated cells (Figure 7C). Interestingly, this
505 phenomenon was not observed when SUM1315MO2 were treated with zeocin. Even to the contrary,
506 zeocin led to even a slight decrease in motility of SUM1315MO2 cells (Figure 7C), suggesting that cells
507 characterized by high HSATII RNA levels are less sensitive to zeocin treatment.
508 As MDA-MB-231, BT-549 and SUM1315MO2 cells are highly metastatic (120, 121), we decided to test
509 effects of HSATII KD on the migratory abilities of these three TNBC cells using the transwell migration
510 (119) and wound healing (122) assays. MDA-MB-231, BT-549 and SUM1315MO2 cells were
511 transfected with either NT-LNA or HSATII-LNAs. 48 h later the motility of cancer cells was assessed, as
512 we previously described (41). Our data demonstrated that HSATII-deficient MDA-MB-231, BT-549 and
513 SUM1315 cells were characterized by significantly lower migratory abilities than control-treated cells
514 with MDA-MB-231 and BT-549 cells (20- and 5-fold decrease, respectively) being the most sensitive to
515 the treatment with HSATII-LNAs (Figure 7D).
516 To perform the wound healing assay, cells were treated with either NT-LNA or HSATII-LNAs and after
517 24 h monolayers of MDA-MB-231, BT-549 and SUM1315MO2 cells were scratched and the closure of

wounds was monitored in time. Similarly to results obtained in the transwell migration, the wound healing assay demonstrated that HSATII-deficient MDA-MB-231, BT-549 and SUM1315 cells were significantly slower in closing wounds compared to control treated cells (Figure 7E).

As the aggressiveness of TNBC cells is also related to their high proliferation rates, we were interested in testing the effects of HSATII KD on the proliferation of MDA-MB-231, BT-549 and SUM1315MO2 cells using the CellTiter 96 AQueous One Solution Cell Proliferation Assay. MDA-MB-231, BT-549 and SUM1315MO2 cells were transfected with either NT-LNA or HSATII-LNAs and 24 h later equal numbers of cells were seeded and cell proliferation monitored for 5 consecutive days. Starting at day 2 for MDA-MB-231 and BT-549 cells and at day 3 post seeding for SUM1315MO2 cells, HSATII RNA KD caused significantly lower proliferation rates when compared with control treated cells (Figure 7F).

Discussion

Satellite repeat transcripts, originating from ubiquitous in human genome SatDNAs, only recently have been described as factors playing important biological roles in chromosome organization and segregation, kinetochore formation as well as heterochromatin regulation (2-5). Many of these ncRNAs, are highly expressed in cancer cells, including HSATII RNA (9, 11), which elevated levels were showed to associate with lower survival of colon cancer patients (15) and its nucleotide CpG-rich sequence was found to be immunostimulatory (12). However, as the expression of some satellite repeat transcripts was triggered by stress, apoptosis, differentiation or cellular senescence (16-18), HSATII induction was indifferent to these cellular programs and was stimulated in colon cancer cells when those cells were only grown in a 3D culture conditions or as xenografts in mice (15), creating technical challenges for studies aimed to investigate mechanisms responsible for the robust elevation of satellite repeat RNAs and their effects on cellular biology.

In our recent report, we demonstrated for the first time that viral infection, specifically infection with HCMV and HSV, significantly induced HSATII RNA, among other satellite repeat transcripts, to the same extent as reported for tumor cells (41). Our studies not only showed that viral infection could be used as a controlled method of inducing satellite repeat RNAs, but allows an expedited interrogation of biological importance of these ncRNAs. Our investigation established that HSATII RNA is an important factor allowing for efficient HCMV infection through its effects on viral gene expression, cellular localization of viral proteins and production of infectious particles (41). Even though, our studies determined HSATII RNA having a broad effect on viral replication cycle in fibroblasts, we noticed that HSATII KD had a somewhat subdued effect of viral DNA accumulation and caused only about 8-fold decrease of viral yield when compared to control infected fibroblasts. Due to high viral titers produced

553 by HCMV-infected fibroblasts, these cells became an infectious cell culture model of choice. However,
554 HCMV infects several cell types, leading often to biologically unique cellular change, thus highlight their
555 specific roles in HCMV pathogenesis (68). While further developing our studies focused on satellite
556 repeat transcripts, we noticed that these unique cellular changes, existing between cell types infected
557 by HCMV, might be also important for the HSATII RNA-based regulation.
558 HCMV infection in epithelial cells was found to be more sensitive to LNA-based knockdown of HSATII
559 RNA (Figure 1) when compared to the effects of HSATII KD in infected fibroblasts (41). Our
560 experiments demonstrated that HSATII RNA deficiencies had a strong negative effect on viral protein
561 levels, accumulation of viral DNA and viral yield, cumulatively accounting for at least 12-20x more
562 potent effect on viral progeny production in ARPE-19 cells when compared to HFFs.
563 We speculate that these clear differences in the strength in which HSATII RNA affects HCMV infection
564 in both cell types are probably multifactorial. Except obvious morphological differences between
565 fibroblasts and epithelial cells (123), the cells were documented to respond differently to extracellular
566 stimuli (124) and to navigate specific splicing programs that lead to diverse makeup of protein isoforms
567 and plausibly an array of differentially regulated biological processes (125). Even though,
568 transcriptomes of fibroblasts and epithelial cells showed to be preferentially concordantly regulated
569 upon HCMV infection, these gene expression profiles were not perfectly overlapping and indicated also
570 some cell specific behavior (126). Additionally, HCMV undergoes different mutational pressures when
571 grown in fibroblast or epithelial cells, as the loss of a broad tropism, production of high titers of cell-free
572 virus and lack of resistance to NK cell-mediated apoptosis are well-documented phenomena seen in
573 fibroblasts (71-73, 127-131). With our previously demonstrated more rapid kinetics of HSATII
574 expression in epithelial cells when compared to fibroblasts (41), our current results provide an
575 additional line of evidence demonstrating differences in response of HSATII RNA between both cell
576 types. Speculatively, it can be hypothesized that differences in protein compositions, related to distinct
577 splicing programs seen in fibroblasts and epithelial cells (125), might lead to differences in their
578 sensitivity to HSATII RNA KD. Therefore, as a more robust system, we chose to use ARPE-19 cells in
579 our investigations focused on identifying molecular mechanism(s) responsible for HSATII induction.
580 Our earlier report described the cooperation between HCMV IE1 and IE2 proteins as necessary for the
581 induction of HSATII RNA expression (41). Based on the IE1- and IE2-driven regulation of Rb and E2F
582 family of proteins, leading to DDR induction and positively affecting HCMV replication (44, 45), we
583 speculated that DDR could be involved in the regulation of HSATII expression. Corresponding with data
584 gather by Bersani *et al.* studying cancer cells (15), our results from epithelial cells demonstrated that
585 HSATII induction is not a blind cellular response to any stressor, as UV-irradiation, oxidative stress or
586 serum withdrawal did not result in a robust HSATII expression, however, these cell stressors inducted
587 the p53 activity as measured by the enhanced expression of CDKN1A and DINO (Figure 2A). Knowing

588 that DNA DSBs were suggested to induce the expression of SINEs (66, 67), we expanded our
589 examination to testing effects of DNA DSBs on HSATII induction. We turned our attention to two DNA
590 damaging agents, zeocin and etoposide, which are known to induce DNA DSBs (84, 85) and, in the
591 case of etoposide, stimulated the expression of mouse B2 SINE RNA (66, 67). Our study demonstrated
592 that not only these chemical compounds induce HSATII RNA in a time-dependent manner similar to the
593 effect of HCMV (Figure 2D ad 2E), but also they provided a novel, well controlled (in a dose-dependent
594 fashion) method of inducing HSATII RNA (Figure 2B and 2C), allowing us to fine-tune the experimental
595 conditions to closely match the strength of HSATII induction seen in HCMV-infected cells to the one
596 produced upon exposing cells to zeocin or etoposide (Figure 2). Therefore, our data not only provided a
597 strong evidence for the DNA DSB-driven DDR response as the trigger of HSATII expression, but also
598 equipped us with an additional, virus-independent, method of analyzing satellite repeat expression.
599 Generated data guided our conclusion that both virus and DNA damaging drugs may utilize the same
600 molecular mechanism to regulate HSATII expression. Therefore, we decided to assess similarities in
601 transcriptomes of HCMV-infected and zeocin-treated cells to lead our further investigation into DDR-
602 mediated satellite repeat expression. Based on our RNA-seq analysis, we uncovered that ~15% of
603 HCMV-regulated genes and ~11% of genes significantly regulated upon zeocin treatment were
604 collectively regulated in both experimental conditions. When those genes were analyzed by GSEA for
605 their association with MSigDB HALLMARK gene sets, we determined that they aligned with
606 G2M_CHECKPOINT, EPITHELIAL_MESENCHYMAL_TRANSITION,
607 INTERFERON_GAMMA_RESPONSE, MTORC1_SIGNALING, DNA_REPAIR, APOPTOSIS gene sets
608 and the most significant overrepresentation seen in E2F_TARGETS gene set (Figure 3), providing an
609 additional support to our notion of the E2F-DDR pathway are involved in HSATII induction. Additionally,
610 we were intrigued that the genes commonly regulated by HCMV and zeocin significantly overlapped
611 with those genes associated with the process of epithelial-to-mesenchymal transition, which correlated
612 with the role of HSATII RNA in cell migration, previously documented by us (41). These results suggest
613 possible unrealized repercussions for cells exposed to DNA damaging agents during chemotherapy
614 and a central role HSAT RNA may play in these responses.
615 In our effort to identify components of DDR pathway important in HSATII induction and being guided by
616 the results of our RNA-seq analysis, we focused our efforts on the E2F family of proteins. Our siRNA-
617 based screen determined that among Rb-regulated factors only siRNA affecting E2F3a and E2F3b
618 RNA levels led to the strong decrease of HSATII RNA in HCMV-infected cells (Figure 4A). The same
619 effect was also seen in IE1/IE2-overexpressing cells (Figure 4B), supporting our hypothesis that DDR
620 induction is triggered by a cooperative action of these two viral proteins and their subsequent effect on
621 Rb/E2F3 ultimately leads to the elevated accumulation of HSATII RNA. Dependent on the biological
622 context, E2F3a and E2F3b were reported to have either contrasting or partially overlapping

transcriptional activities (46, 47, 95-98). Thus, it became important to identify what contributions both E2F3 isoforms have to HSATII expression. Our results showed that among E2F1, E2F2 and E2F3s, only E2F3a, which is classically considered a transcriptional activator, positively influenced HSATII expression (Figure 4C). Importantly, E2F3a was not only elevated in HCMV-infected, but also in zeocin- and etoposide-treated cells (Figure 4D), suggesting that even though DNA damaging drugs directly effect DNA stability and induce DDR pathway, especially in case of etoposide treatment, the elevated expression of E2F3a can contribute to the overall accumulation of HSATII RNA in treated cells. Interestingly, when we analyzed E2F3a protein levels in HCMV-infected and IE1/IE2-expressing cells, the kinetics of HSATII expression did not correlated with the abundance of E2F3a in these cells, as the protein was detected at later times post infection (Figure 4E). On the other hand, E2F3a seemed to be constitutively expressed in IE1/IE2-expressing cells (Figure 4E) and those cells are characterized by a slower HSATII kinetics when compared to infected cells (41). Therefore, we speculate that E2F3a is not solely responsible for HSATII induction and other unidentified transcription factors might be important for the high expression of HSATII seen in HCMV-infected and DNA damaging drug-treated cells.

To conclusively associate E2F3-driven regulation to HSATII expression, we demonstrated that E2F3 siRNA significantly decreased the expression of most viral transcripts tested (Figure 4F), providing an important connection between E2F3/DDR-driven HSATII induction, viral gene expression regulated by this satellite repeat transcript (41) and its ultimate effect on viral progeny production, as showed by an increased viral load produced by cells treated with zeocin (Figure 4G).

The question remains why E2F3a, but not other Rb-regulated E2Fs, such as E2F1 and E2F2, specifically drives HSATII expression. E2F1 was previously showed to contribute to the DDR induction and to aid to HCMV replication, but neither E2F2 nor E2F3a/b were showed to affect HCMV yield (132). We suggest that these discrepancies might be related to differences in cell types used and, additionally, we determined that it was critical for enhancing siRNA KD efficiency to extend siRNA treatment to 2-3 days before infecting cells, as these conditions allowed for efficient KDs and to appreciate siRNA effects on HSATII expression and viral yields.

Seeing the specificity of E2F3a in driving HSATII expression and a favorable environment for viral infection in cells with the activated DNA DSB-based DDR, it became even more important to determine what aspects of DDR lead to HSATII expression and ultimately efficient viral replication.

Depending on the type of DNA damage different arms of DDR are activated, including ATM-, ATR- or DNA-PK-based pathways (58, 60, 105).

Our data collaborated with an earlier study, which investigated a role of DDR in HCMV-infected cells (132), as we demonstrated that both HCMV and zeocin lead at 24 hpi/hpt to increased phosphorylation of H2AX histone. However, it needs to be noted that zeocin had a much stronger effect on H2AX phosphorylation than HCMV infection (Figure 5A and 5B), which could be explained by a more direct

658 effect of the drug on DNA stability and faster kinetics of DDR response in zeocin-treated cells. Knowing
659 that both HCMV and zeocin trigger the accumulation of γ-H2AX and our results strongly supported the
660 importance of DNA DSBs in HSATII expression, we hypothesized that ATM pathway is the most
661 probable DDR response that could influence the induction of satellite repeat transcripts. Our siRNA-
662 based screen strongly supported this notion as either in HCMV-infected or in zeocin-treated cells only
663 ATM KD, and not ATR or DNA-PK KDs, resulted in substantial downregulation of HSATII expression
664 (Figure 5C and 5D). An additional confirmation of a central role of ATM in HSATII induction came also
665 from our studies performed on HCMV-infected, zeocin- or etoposide-treated ataxia-telangiectasia
666 fibroblasts. In each experimental condition tested, cells with mutated ATM gene were characterized by
667 significantly lower levels of HSATII RNA when compared to cells expressing a functional ATM protein
668 (Figure 5E). Therefore, our investigation uncovered a novel regulatory mechanism, in which ATM
669 governs the induction of HSATII RNA and through this effect on the satellite repeat expression
670 positively influences HCMV replication, providing a molecular explanation to the ATM role during HCMV
671 infection reported by Xiaofei et al. (132). Surprisingly, when we tried to specifically assess the role of
672 ATM kinase activity by inhibiting its function with two specific inhibitors, Ku-55933 and AZ31 (108, 109),
673 cells treated with these chemical compounds did not respond with a lower expression of HSATII (Figure
674 5F). However, as suspected both treatments negatively affected expression of CDKN1A and DINO
675 transcripts when compared to control cells (Figure 5F), suggesting that ATM kinase activity is
676 dispensable in the regulation of HSATII expression.
677 In support to the ATM-based but its kinase-independent effect on HSATII induction, we also determined
678 that at 24 h and 120 h post HCMV infection or zeocin treatment ATM-regulated Chk1, Chk2 or p53
679 showed no effect on HSATII expression (Figure 6A, 6D and 6E). However, zeocin at both tested times
680 and HCMV late in infection showed stimulation of the p53 activity (Figure 6B and 6C).
681 Together, our data suggest a specific bypassing of ATM function away from its canonical kinase-based
682 activity for the induction of HSATII.
683 Interestingly, ATM was reported to have DDR-independent roles, including its regulation of glucose
684 metabolism (133) and NF-κB activity (134) - both processes tightly associated with HCMV infection
685 (135-143). Moreover, ATM kinase-independent function was described for ATM interacting with E3
686 ubiquitin ligase during the induction of mitophagy (141). As the mitochondrial homeostasis is central for
687 HCMV replication (144-146), ATM kinase-independent induction of HSATII expression may provide an
688 unappreciated link to molecular regulation of these processes.
689 Notably, glucose metabolism, NF-κB activity and mitophagy play important roles in cancer biology (147-
690 152). Additionally, E2Fs are highly expressed in breast cancers, E2F3a was demonstrated to stimulate
691 cell proliferation and carcinogenesis (98, 153) and ATM has multiple effects on cancer cell biology
692 (154). Together with the knowledge that a high HSATII expression was detected in several cancers (9,

693 11), HSATII levels correlated with survival of cancer patients (15) and satellite repeat transcripts in
694 blood plasma have been considered as tumor markers (155, 156), we had a strong belief that HSATII
695 RNA may play an important role in biology of cancer cells and that the use of DNA damaging drugs
696 may provide, thorough elevated levels of HSATII RNA, a favorable environment aiding to
697 oncomodulatory processes.
698 Breast cancers are a leading cause of cancer-related mortality in women (53) and a presence of HCMV
699 has been reported in several cancers, including breast cancer (39, 157-160). By assessing HSATII
700 expression levels in breast cancer cell lines characterized by varying degree of p53 status, hormonal
701 dependency and tumor aggressiveness, we determined that there was a tendency of highly metastatic
702 breast cancer cells to have enhanced induction of HSATII expression compared to cells with a less
703 invasive phenotype and wild type status of p53 (Figure 7A). Importantly, we also uncovered that breast
704 cancer cells, independently to their initial levels of HSATII RNA, were prone to induce a robust
705 expression of satellite repeats upon zeocin treatment (Figure 7B). However, only cells characterized by
706 a low basal expression of HSATII RNA, i.e. ARPE-19 and MCF-7 cells, showed enhanced migratory
707 phenotype when exposed to zeocin (Figure 7C), supporting our previous report describing the role of
708 HSATII RNA in enhanced migration of HCMV-infected cells (41) and suggesting that the level of
709 HSATII RNA may determine the fate of cells upon their exposure to DNA damaging agents. These
710 results prompt to speculate that a wide usage of DNA damaging agents as chemotherapeutics may
711 lead to unforeseen HSATII RNA-based oncomodulatory processes in non- or pre-cancerous cells.
712 Importantly, these therapies often lead to drug resistance (55, 56) and raise concerns about a
713 development of *de novo* primary tumors (57), highlighting a possible role of overexpressed HSATII
714 RNA in these clinical disease manifestations. Even though, zeocin treatment was not able to enhanced
715 migration of already highly invasive SUM1315MO2, our studies showed a very strong reliance of
716 metastatic MDA-MB-231, BT-549 and SUM1315MO2 cells on HSATII RNA-based regulation for their
717 migratory phenotype (Figure 7D and 7E) and for their high proliferative capabilities (Figure 7F),
718 suggesting HSATII RNA as a potential candidate for anti-cancer treatments.
719 Significant progress has been made in increasing the arsenal of effective anti-cancer drugs, including
720 DNA damaging agents (55, 56). However, the toxicity and temporary remissions that are common for
721 these drugs (55, 56), highlight the need for a comprehensive understanding of biological mechanisms
722 regulated by DNA damaging agents. It is tempting to speculate that DNA damaging agents could have
723 a broad stimulatory effect on the expression of satellite repeats in exposed cells, changing cellular
724 regulatory pathways and ultimately leading to oncogenic changes in those cells.
725 The use of viruses or DNA damaging agents provides a inducible and highly controlled cellular systems
726 that allow detailed analysis of the roles of these ncRNAs play in normal and cancer cells.

727 Together with the knowledge that E2F3a stimulates cell proliferation and carcinogenesis (98, 153) and
728 ATM has multiple effects on cancer cell biology (154), our investigation provides the molecular
729 mechanism that links a high expression of HSATII RNA to the E2F3a-initiated induction of DDR,
730 centered around kinase-independent functions of ATM, and to processes critical for efficient viral
731 infection, cancer cell migration and proliferation.
732 Therefore, our studies uncover several therapeutic targets that could be use in efforts to develop novel
733 antiviral and anticancer interventions.
734
735
736 **Methods**
737
738 **Cells, viruses and drugs.** Human retinal pigment epithelial (ARPE-19) (25) and breast epithelial
739 (MCF-10A) cells as well as breast cancer cell lines: MCF-7, MDA-MB-175VII, MDA-MB-361, and MDA-
740 MB-231 were from the American Type Culture Collection (ATCC). SUM1315MO2 breast cancer cells
741 (161) were generously provided by Stephen Ethier (Medical University of South Carolina). A-T (-)
742 fibroblasts, originally named AT22IJE-T, and A-T (+) fibroblasts with a stably expressed functional ATM
743 were created by the lab of Yosef Shiloh (Sackler School of Medicine) (106, 107) and generously
744 provided by Matthew Weitzman (Perelman School of Medicine University of Pennsylvania). ARPE-19,
745 MCF-7, MDA-MB-175VII, MDA-MB-361, MDA-MB-231 and SUM1315MO2 cells were cultured in 10%
746 FBS/DMEM with added Ham's F-12 nutrient mixture (Sigma-Aldrich) and supplemented with 1x MEM
747 Non-Essential Amino Acids Solution (ThermoFisher Sceintific), 1 mM sodium pyruvate (ThermoFisher
748 Sceintific), 1x GlutaMAX (ThermoFisher Sceintific) and 10 mM Hepes, pH 7.4 (ThermoFisher
749 Sceintific). A-T (-) and A-T (+) cells were cultured in 10% FBS/DMEM. Media were supplemented with
750 penicillin G sodium salt (100 units/ml; Sigma-Aldrich) and streptomycin sulfate (95 units/ml; Fisher
751 Scientific). IE1 and IE2-expressing ARPE-19 cells were described previously (41).
752 BAC infectious clone of HCMV strain TB40/E-GFP (TB40/Ewt-GFP) (162) was electroporated into
753 human foreskin fibroblasts (HFF) or ARPE-19 cells to generate viral progeny that were propagated
754 once more in HFFs or ARPE-19 cells, respectively. TB40/E-GFP-epi designates TB40/E-GFP virus
755 grown in ARPE-19 cells (163). All viral stocks were partially purified by centrifugation through a 20% D-
756 sorbitol cushion in buffer containing 50 mM Tris·HCl, 1 mM $MgCl_2$, pH 7.2, resuspended in DMEM and
757 stored in aliquots at -80°C. Infections were performed by treating cells with viral inoculum for 2 h,
758 followed by removal of the inoculum and washing with phosphate-buffered saline (PBS; Sigma-Aldrich)
759 before applying fresh medium. To quantify extracellular virions, media from infected cells was collected,
760 spun down for 10 min. at 2000 x g. To quantify intracellular virions, infected cells were washed with
761 PBS, scrapped and intracellular virus released by 3 rounds of freezing and thawing. Samples were

762 spun down for 10 min. at 2000 x g. Viral stocks and sample supernatant were titered by either the
763 $TCID_{50}$ method (164) or plaque assay.
764 Zeocin (InvivoGen) was dissolved in water and stored at -20°C. Etoposide (Millipore Sigma), Ku-55933
765 (Tocris) and AZ31 (Selleckchem) were dissolved in DMSO and stored at -20°C.
766
767 **RNA sequence analysis (RNA-seq).** RNA was collected in QIAzol Lysis Reagent (Qiagen) and
768 isolated using the miRNeasy Mini Kit (Qiagen). DNA was removed from samples using Turbo DNase
769 (Thermo Fisher Scientific) and RNA quality was assessed using the Bioanalyzer 2100 (Agilent
770 Technologies). Sequencing libraries were prepared using the TruSeq Stranded Total RNA with Ribo-
771 Zero kit (Illumina), and sequenced on Illumina HiSeq2500 sequencer instrument in paired-end, rapid
772 mode (2x 150bp).
773 For the RNA-seq analysis, the Galaxy instance of Princeton University was used (165). RNA-Seq data
774 was de-multiplexed based on indexes. Phred quality scores were checked by using the FastQC toolkit
775 and were greater than 26 for more than 90% of the read length. Human and HCMV fasta and
776 annotation (.gtf) files were created for mapping by combining sequences and annotations from Ensembl
777 annotation, build 38 and TB40 (EF999921). Reads were mapped to the concatenated human-virus
778 genomes using RNA STAR (86) (Galaxy version 2.6.0b-2). The featureCounts (166) (Galaxy version
779 1.6.4) was used to measure gene expression. The resulting files were used as input to determine
780 differential expression for each gene utilizing DESeq2 (167) (Galaxy version 2.11.40.6). Fold changes
781 in gene expression were considered significant when the adjusted *P* value (q value) for multiple testing
782 with the Benjamini–Hochberg procedure, which controls FDR, was <0.05.
783 To visualize read coverage tracks for alignment files, RNA STAR-generated BAM files were imported
784 into the Integrative Genomics Viewer (168) (IGV; version 2.6.3) and aligned with human genome
785 assembly hg19 focused on the HSATII locus on chromosome 16. The scale of read coverage peaks
786 was adjusted for experimentally paired samples.
787 To create Venn diagrams, based on data from the DESeq2 analysis the list of significantly expressed
788 genes in HCMV-infected or zeocin-treated cells compared to control cells were imported into a web-
789 based tool InteractiVenn (169).
790 Gene Set Enrichment Analysis (GSEA) (87) was used to the list of common genes differentially
791 expressed in both HCMV-infected and zeocin-treated cells using the hallmark gene set of the Molecular
792 Signature Database (MSigDB) (88). A matrix of differentially expressed genes from the data set
793 significantly matching the hallmark gene set of MSigDB was composed and a list of the hallmark gene
794 subsets was ordered based on a number of overlapping genes, *p* value determining the probability of
795 association with a given gene set and a false discovery rate q-value.
796

797 **Quantification of nucleic acid.** For analysis of RNA by qRT-PCR, RNA was extracted from samples
798 collected in QIAzol lysis reagent using the miRNeasy kit (Qiagen). cDNA was made from 1 mg of total
799 RNA with random hexamer primers and MultiScribe reverse transcriptase (Applied Biosystems),
800 according to the manufacturer`s protocol. Transcript specific primer sequences used in the study were
801 either previously reported (41) or newly designed primer sets are as follow: CDKN1A Forward 5'-
802 TTTAACAGCCTGCTCCCTTG-3', Reverse 5'-AGTTTGCAACCATGCACTTG-3'; DINO Forward 5'-
803 GGAGGCAAAAGTCCTGTGTT-3', Reverse 5'-GGGCTCAGAGAAGTCTGGTG-3'; E2F1 Forward 5'-
804 CCGTGGACTCTTCGGAGAAC-3', Reverse 5'-ATCCCACCTACGGTCTCCTC-3'; E2F2 Forward 5'-
805 TGGGTAGGCAGGGGAATGTT-3', Reverse 5'-GCCTTGTCCTCAGTCAGGTG-3'; E2F3a Forward 5'-
806 TTTAAACCATCTGAGAGGTACTGATGA-3', Reverse 5'-CGGCCCTCCGGCAA-3'; E2F3b Forward 5'-
807 TTTAAACCATCTGAGAGGTACTGATGA-3', Reverse 5'- CCCTTACAGCAGCAGGCAA-3'; E2F4
808 Forward 5'-TGGAAGGTATCGGGCTAAT-3', Reverse 5'-CAATCAGTTTGTCAGCAATCTC-3'; E2F5
809 Forward 5'-CGGCAGATGACTACAACTTTA-3', Reverse 5'-GATAACAGTCCCAAGTTTCCA-3'; ATM
810 Forward 5'-GCACTGAAAGAGGATCGTAAA-3', Reverse 5'-GAGGGAACAAAGTCGGAATAC-3'; ATR
811 Forward 5'-ATATCACCCAAAAGGCGTCGT-3', Reverse 5'-TGCTCTTTTGGTTCATGTCCAC-3';
812 PRKDC Forward 5'-AAATGGGCCAGAAGATCGCA-3', Reverse 5'-AGGTCCAGGGCTGGAATTTT-3';
813 CHEK1 Forward 5'-TTTGGACTTCTCTCCAGTAAAC-3', Reverse 5'-GCTGGTATCCCATAAGGAAAG-
814 3'; CHEK2 Forward 5'-CGCGGTCGTGATGTCTCGGG-3', Reverse 5'-CGCTGCCATGGGGCTGTGAA-
815 3'; TP53 Forward 5'-AGGGATGTTTGGGAGATGTAAG-3', Reverse 5'-
816 CCTGGTTAGTACGGTGAAGTG-3'. qPCR was performed using SYBR Green master mix (Applied
817 Biosystems) on a QuantStudio™ 6 Flex Real-Time PCR System (Applied Biosystems). Transcript levels
818 were analyzed using the DDCt method and GAPDH was used as an internal control (170). Error ranges
819 are reported as standard deviation of the mean (SD).
820
821 For quantification of viral DNA accumulation in infected cells, cells were harvested and intracellular
822 DNA was isolated using the DNA Blood & Tissue Kit (Qiagen). DNA was RNase A treated (2 mg/ml;
823 Qiagen) and viral DNA was quantified by qPCR using primers specific for the viral genomic UL44
824 (Forward: 5'-GTGCGCGCCCGATTTCAATATG-3', Reverse: 5'-GCTTTCGCGCACAATGTCTTGG-3')
825 or cellular genomic GAPDH (Forward: 5'-CCCCACACACATGCACTTACC-3', Reverse: 5'-
826 CCTAGTCCCAGGGCTTTGATT-3').
827
828 **Analysis of proteins.** For Western blot analysis, cells were harvested using lysis buffer (50 mM Tris-
829 HCl, pH 7.5, 5 mM EDTA, 100 mM NaCl, 1% Triton X-100, 0.1% SDS, and 10% glycerol). Samples
830 were mixed with 6xSDS sample buffer (325 mM Tris pH 6.8, 6% SDS, 48% glycerol, 0.03%
831 bromophenol blue containing 9% 2-mercaptoethanol). Proteins were separated by electrophoresis

832 (SDS-PAGE) and transferred to ImmunoBlot polyvinylidene difluoride (PVDF) membranes (BioRad
833 Laboratories). Western blot analyses were performed using primary antibodies recognizing cellular
834 proteins: E2F3 (clone PG30; Santa Cruz Biotechnology) and β-actin (clone AC-15; Abcam), or HCMV
835 proteins: IE1 [clone 1B12 (171)], IE2 [clone 3A9 (172)], pUL44 (clone 10D8; Virusys), pUL69 [clone
836 10E11 (173)], pp71 [clone 2H10-9 (174)] and pp28 [clone 10B4 (175)]. Goat anti-mouse (GE
837 Healthcare Biosciences) conjugated with horseradish peroxidase was used as a secondary antibody.
838 Western blots were developed using WesternSure ECL Detection Reagents (Licor).
839 For immunofluorescence assays, ARPE-19 cells grown in 96-well plates were infected with TB40/E-
840 GFP-epi (3 IU/cell), treated with zeocin (200 mg/mL) or left untreated. After 24 h, cells were fixed in
841 100% methanol (Sigma) and incubated in blocking solution [PBS with 3% bovine serum albumin (BSA;
842 Fisher Scientific) prior to the addition of a primary mouse monoclonal antibody specific for phospho-
843 Histone H2AX (Ser13; clone JBW301; Millipore Sigma). Following incubation, cells were washed with
844 PBS, and a donkey Alexa488-conjugated anti-mouse secondary antibody (Santa Cruz Biotechnology)
845 was applied. Nuclei were counterstained with the Hoechst stain. Cells were visualized and % of γ-
846 H2A.X-positive cells was calculated using the Operetta high-content imaging and analysis system
847 (PerkinElmer; Waltham, MA) with 20X objective.
848
849 **Plasmid transfection.** Plasmids used in the study: pCMV-Neo-Bam was a gift from Bert Vogelstein
850 (Addgene plasmid #16440). pCMV-Neo-Bam E2F3a and pCMV-Neo-Bam E2F3b were gifts from
851 Jacqueline Lees (Addgene plasmid #37970 and #37970, respectively). pCMVHA E2F1 and pCMVHA
852 E2F2 were gifts from Kristian Helin (Addgene plasmids #24225 and #24226, respectively).
853 ARPE-19 cells at 70-80% confluency were transfected with 1 µg of each plasmid using Lipofectamine
854 3000 (ThermoFischer Scientific) according to the manufacturer's instructions. 72 h later, plasmid-
855 transfected cells were harvested using TRIzol and samples were stored at -80°C.
856
857 **Cell stress induction.** For the serum deprivation stress (176), cells were washed with 1xPBS,
858 supplemented with media lacking FBS and cultured for 24 h. For the oxidative stress (177), cells were
859 washed with 1xPBS, supplemented with media lacking FBS, but containing 100 μM of H_2O_2 and
860 cultured for 24 h. For UV-irradiation-based stress (178), cells were washed with 1xPBS, exposed to the
861 ultra violet light (50 J/m^2) using a Stratalinker (Stratagene), washed with 1xPBS, supplemented with
862 10%FBS/DMEM and cultured for 24 h.
863
864 **HSATII RNA knockdown.** Locked nucleic acid (LNA™; Exiqon, Skelstedt, Denmark) oligonucleotides
865 targeting HSATII RNA were described previously (41). Shortly, HSATII-LNA #1, HSATII-LNA #2 or a
866 mixture of both (HSATII-LNAs #1+#2) were used for experiments as indicated. Lipofectamine

867 RNAiMAX® Reagent (Thermo Fisher Scientific, Waltham, MA) and LNAs were resuspended in Opti-
868 MEM® medium (Thermo Fisher Scientific) according to the manufacturer's instructions. Non-target LNA
869 (NT-LNA) was used as a negative control. ARPE-19 cells were incubated for 24-48 h before being
870 subjected to subsequent experimental procedures.
871
872 **siRNA knockdown.** siRNAs targeting E2F1 (E2F1 siRNA), E2F2 (E2F2 siRNA), E2F3 (E2F3 siRNA),
873 E2F4 (E2F4 siRNA), E2F5 (E2F5 siRNA), CHEK1 (CHEK1 siRNA) and CHEK2 (CHEK2 siRNA) were
874 ordered as siGENOME SMARTpools (Dharmacon). siRNAs targeting ATM (ATM siRNA), ATR (ATR
875 siRNA), PRKDC (DNA-PK siRNA) and TP53 (TP53 siRNA) were ordered as ON-TARGETplus
876 SMARTpools (Dharmacon). All siRNAs and appropriate NT siRNAs (siGENOME Non-targeting siRNA
877 Pool #1 and ON-TARGETplus Non-targeting Control Pool; Dharmacon) were purchased from Life
878 Technologies. ARPE-19 cells were grown to ~80% confluence and then transfected with siRNA using
879 Lipofectamine® RNAiMAX Reagent (Life Technologies). Cells transfected with non-specific, scrambled
880 siRNA (NT siRNA) (Life Technologies) served as a negative control. Following 24 h incubation with
881 siRNA, cells were washed with 1xPBS and subjected to subsequent experimental procedures.
882
883 **Cell migration assays.** Wound healing assays were performed as described previously (41). Shortly,
884 confluent monolayers of NT-LNA- or HSATII-LNA-transfected MDA-MB-231, BT-549 and
885 SUM1315MO2 cells were scratched with a 1-ml pipet to create wounds. The process of wound closure
886 was monitored in time using the Nikon Eclipse TE2000-U inverted microscope. The average wound
887 width (in arbitrary units) of ARPE-19 cells was calculated from 6 measurements for each experimental
888 arm from the captured images using ImageJ software (179). Results are plotted as a mean percent of
889 remaining wound width (SD).
890 Transwell migration assays were performed as described previously (41). Shortly, NT-LNA- or HSATII-
891 LNA -transfected MDA-MB-231, BT-549 and SUM1315MO2 or zeocin-treated ARPE-19, MCF-7 and
892 SUM1315MO2 cells were trypsinized and equal number of cells seeded onto each filter in FBS-free
893 medium containing ITS Liquid Media Supplement (Sigma-Aldrich). After 24 h, filters were washed, cells
894 were fixed. and migrated cells on the bottom surface of the filter were stained with 0.2% crytal violet
895 solution. Migrated cells were imaged and quantified using ImageJ software (179).
896
897 **Cell proliferation assay.** Cells were transfected with NT-LNA or HSATII-LNAs. After 48 hpt, equal
898 number of cells (2500 cells/well) were seeded into 96-well plates and cultured in 10% FBS/DMEM with
899 added Ham's F-12 nutrient mixture and supplemented with 1x MEM Non-Essential Amino Acids
900 Solution, 1 mM sodium pyruvate, 1x GlutaMAX and10 mM Hepes, Cell proliferation was monitored
901 using a colorimetric CellTiter 96 AQueous One Solution Cell Proliferation Assay according to the

902 manufacturer's protocol. Absorbance was measured at 490 nm using the SpectraMax Plus 384
903 Microplate reader (Molecular Devices, Sunnyvale, CA).
904
905 **Cell toxicity assay.** ARPE-19 cells were treated with zeocin, etoposide, Ku-55933 or AZ31 at specified
906 range of concentrations for 24h or either water or DMSO as solvent controls. Each tested concentration
907 of specific drug contained the same concentration of solvent. At indicated time points, the Cell Titer
908 96® AQueous One Solution Cell Proliferation Assay (Promega, Madison, WI) was performed according
909 to the manufacturer's instructions. Absorbance was measured at 490 nm using the SpectraMax Plus
910 384 Microplate reader (Molecular Devices, Sunnyvale, CA).
911
912 **Statistical analysis.** To determine statistical significance among samples in experiments, an unpaired,
913 two-tailed *t*-tests Welch`s correction were performed between the arrays of data from distinct samples
914 to determine *P* values. *P* value <0.05 was considered significant. Significance is shown by the
915 presence of asterisks above data points with one, two, three or four asterisks representing *P*<0.05,
916 *P*<0.01, *P*<0.001 or P<0.0001, respectively. Only significant *P* values are reported.
917
918 **Data availability.** Raw RNA-seq data will be available from the NCBI Gene Expression Omnibus
919 (GEO). All relevant experimental data are available from the authors.
920
921
922 ## Acknowledgments
923
924 We would like to thank Stephen Ethier (Medical University of South Carolina) for generously providing
925 SUM1315MO2 cells; Matthew Weitzman (Perelman School of Medicine University of Pennsylvania) for
926 generously providing A-T (-) and A-T (+) fibroblasts, A. Oberstein (University of Illinois) for creating
927 IE1/IE2-expressing ARPE-19 cells and members of the T.S. laboratory for scientific discussions.
928
929 This work was supported by National Institutes of Health Grant AI112951. M.T.N. was partially
930 supported by American Cancer Society Fellowship PF-14-116-01-MPC.
931
932
933 ## References
934
935 1. Levine AJ, Ting DT, & Greenbaum BD (2016) P53 and the defenses against genome instability
936 caused by transposons and repetitive elements. *Bioessays* 38(6):508-513.
937

2. Pezer Z, Brajkovic J, Feliciello I, & Ugarkovc D (2012) Satellite DNA-mediated effects on genome regulation. *Genome Dyn* 7:153-169.

3. Eymery A*, et al.* (2009) A transcriptomic analysis of human centromeric and pericentric sequences in normal and tumor cells. *Nucleic Acids Res* 37(19):6340-6354.

4. Hall LE, Mitchell SE, & O'Neill RJ (2012) Pericentric and centromeric transcription: a perfect balance required. *Chromosome Res* 20(5):535-546.

5. Garrido-Ramos MA (2017) Satellite DNA: An Evolving Topic. *Genes (Basel)* 8(9).

6. Gronbaek K, Hother C, & Jones PA (2007) Epigenetic changes in cancer. *APMIS* 115(10):1039-1059.

7. Kanwal R & Gupta S (2012) Epigenetic modifications in cancer. *Clin Genet* 81(4):303-311.

8. Sanchez Calle A, Kawamura Y, Yamamoto Y, Takeshita F, & Ochiya T (2018) Emerging roles of long non-coding RNA in cancer. *Cancer Sci* 109(7):2093-2100.

9. Ting DT*, et al.* (2011) Aberrant overexpression of satellite repeats in pancreatic and other epithelial cancers. *Science* 331(6017):593-596.

10. Leonova KI*, et al.* (2013) p53 cooperates with DNA methylation and a suicidal interferon response to maintain epigenetic silencing of repeats and noncoding RNAs. *Proc Natl Acad Sci U S A* 110(1):E89-98.

11. Hall LL*, et al.* (2017) Demethylated HSATII DNA and HSATII RNA Foci Sequester PRC1 and MeCP2 into Cancer-Specific Nuclear Bodies. *Cell reports* 18(12):2943-2956.

12. Tanne A*, et al.* (2015) Distinguishing the immunostimulatory properties of noncoding RNAs expressed in cancer cells. *Proc Natl Acad Sci U S A* 112(49):15154-15159.

13. Bogunovic D*, et al.* (2009) Immune profile and mitotic index of metastatic melanoma lesions enhance clinical staging in predicting patient survival. *Proc Natl Acad Sci U S A* 106(48):20429-20434.

14. Cosset E*, et al.* (2014) Comprehensive metagenomic analysis of glioblastoma reveals absence of known virus despite antiviral-like type I interferon gene response. *Int J Cancer* 135(6):1381-1389.

15. Bersani F*, et al.* (2015) Pericentromeric satellite repeat expansions through RNA-derived DNA intermediates in cancer. *Proc Natl Acad Sci U S A* 112(49):15148-15153.

16. Valgardsdottir R*, et al.* (2008) Transcription of Satellite III non-coding RNAs is a general stress response in human cells. *Nucleic Acids Res* 36(2):423-434.

17. Bouzinba-Segard H, Guais A, & Francastel C (2006) Accumulation of small murine minor satellite transcripts leads to impaired centromeric architecture and function. *Proc Natl Acad Sci U S A* 103(23):8709-8714.

18. De Cecco M*, et al.* (2013) Genomes of replicatively senescent cells undergo global epigenetic changes leading to gene silencing and activation of transposable elements. *Aging Cell* 12(2):247-256.

19. Mesri EA, Feitelson MA, & Munger K (2014) Human viral oncogenesis: a cancer hallmarks analysis. *Cell Host Microbe* 15(3):266-282.

20. Krump NA & You J (2018) Molecular mechanisms of viral oncogenesis in humans. *Nat Rev Microbiol* 16(11):684-698.

21. Zhu Q*, et al.* (2011) BRCA1 tumour suppression occurs via heterochromatin-mediated silencing. *Nature* 477(7363):179-184.

22. Michaelis M, Doerr HW, & Cinatl J (2009) The story of human cytomegalovirus and cancer: increasing evidence and open questions. *Neoplasia* 11(1):1-9.

23. Herbein G (2018) The Human Cytomegalovirus, from Oncomodulation to Oncogenesis. *Viruses* 10(8).

24. Lepiller Q, Aziz Khan K, Di Martino V, & Herbein G (2011) Cytomegalovirus and tumors: two players for one goal-immune escape. *The open virology journal* 5:60-69.

25. Vastag L, Koyuncu E, Grady SL, Shenk TE, & Rabinowitz JD (2011) Divergent effects of human cytomegalovirus and herpes simplex virus-1 on cellular metabolism. *PLoS Pathog* 7(7):e1002124.

26. Kumari P*, et al.* (2017) Essential role of HCMV deubiquitinase in promoting oncogenesis by targeting anti-viral innate immune signaling pathways. *Cell Death Dis* 8(10):e3078.

27. Collins-McMillen D*, et al.* (2015) Human Cytomegalovirus Promotes Survival of Infected Monocytes via a Distinct Temporal Regulation of Cellular Bcl-2 Family Proteins. *J Virol* 90(5):2356-2371.

28. Sia IG & Patel R (2000) New strategies for prevention and therapy of cytomegalovirus infection and disease in solid-organ transplant recipients. *Clin Microbiol Rev* 13(1):83-121.

29. Kanj SS, Sharara AI, Clavien PA, & Hamilton JD (1996) Cytomegalovirus infection following liver transplantation: review of the literature. *Clin Infect Dis* 22(3):537-549.

30. Gerna G*, et al.* (2012) Human cytomegalovirus end-organ disease is associated with high or low systemic viral load in preemptively treated solid-organ transplant recipients. *New Microbiol* 35(3):279-287.

31. Lanzieri TM, Dollard SC, Bialek SR, & Grosse SD (2014) Systematic review of the birth prevalence of congenital cytomegalovirus infection in developing countries. *Int J Infect Dis* 22:44-48.

32. Bissinger AL, Sinzger C, Kaiserling E, & Jahn G (2002) Human cytomegalovirus as a direct pathogen: correlation of multiorgan involvement and cell distribution with clinical and pathological findings in a case of congenital inclusion disease. *J Med Virol* 67(2):200-206.

33. Soroceanu L & Cobbs CS (2011) Is HCMV a tumor promoter? *Virus Res* 157(2):193-203.

1040
1041 34. Bhattacharjee B, Renzette N, & Kowalik TF (2012) Genetic analysis of cytomegalovirus in
1042 malignant gliomas. *J Virol* 86(12):6815-6824.
1043
1044 35. El-Shinawi M*, et al.* (2013) Human cytomegalovirus infection enhances NF-kappaB/p65
1045 signaling in inflammatory breast cancer patients. *PLoS One* 8(2):e55755.
1046
1047 36. Michaelis M*, et al.* (2012) Selection of a highly invasive neuroblastoma cell population through
1048 long-term human cytomegalovirus infection. *Oncogenesis* 1:e10.
1049
1050 37. Ranganathan P, Clark PA, Kuo JS, Salamat MS, & Kalejta RF (2012) Significant association of
1051 multiple human cytomegalovirus genomic Loci with glioblastoma multiforme samples. *J Virol*
1052 86(2):854-864.
1053
1054 38. Harkins L*, et al.* (2002) Specific localisation of human cytomegalovirus nucleic acids and
1055 proteins in human colorectal cancer. *Lancet* 360(9345):1557-1563.
1056
1057 39. Harkins LE*, et al.* (2010) Detection of human cytomegalovirus in normal and neoplastic breast
1058 epithelium. *Herpesviridae* 1(1):8.
1059
1060 40. Cinatl J, Scholz M, Kotchetkov R, Vogel JU, & Doerr HW (2004) Molecular mechanisms of the
1061 modulatory effects of HCMV infection in tumor cell biology. *Trends Mol Med* 10(1):19-23.
1062
1063 41. Nogalski MT*, et al.* (2019) A tumor-specific endogenous repetitive element is induced by
1064 herpesviruses. *Nat Commun* 10(1):90.
1065
1066 42. Whitley RJ (1996) Herpesviruses. *Medical Microbiology*, eds th & Baron SGalveston (TX)).
1067
1068 43. Alibek K*, et al.* (2014) Implication of human herpesviruses in oncogenesis through immune
1069 evasion and supression. *Infect Agent Cancer* 9(1):3.
1070
1071 44. Xiaofei E & Kowalik TF (2014) The DNA damage response induced by infection with human
1072 cytomegalovirus and other viruses. *Viruses* 6(5):2155-2185.
1073
1074 45. Xiaofei E*, et al.* (2012) RNA interference-mediated targeting of human cytomegalovirus
1075 immediate-early or early gene products inhibits viral replication with differential effects on
1076 cellular functions. *J Virol* 86(10):5660-5673.
1077
1078 46. DeGregori J & Johnson DG (2006) Distinct and Overlapping Roles for E2F Family Members in
1079 Transcription, Proliferation and Apoptosis. *Curr Mol Med* 6(7):739-748.
1080
1081 47. Lammens T, Li J, Leone G, & De Veylder L (2009) Atypical E2Fs: new players in the E2F
1082 transcription factor family. *Trends Cell Biol* 19(3):111-118.
1083
1084 48. Chen HZ, Tsai SY, & Leone G (2009) Emerging roles of E2Fs in cancer: an exit from cell cycle
1085 control. *Nat Rev Cancer* 9(11):785-797.
1086
1087 49. Nevins JR (2001) The Rb/E2F pathway and cancer. *Hum Mol Genet* 10(7):699-703.
1088
1089 50. Sherr CJ & McCormick F (2002) The RB and p53 pathways in cancer. *Cancer Cell* 2(2):103-
1090 112.
1091

1092 51. Ren B*, et al.* (2002) E2F integrates cell cycle progression with DNA repair, replication, and
1093 G(2)/M checkpoints. *Genes Dev* 16(2):245-256.
1094
1095 52. Zhu Q*, et al.* (2018) Heterochromatin-Encoded Satellite RNAs Induce Breast Cancer. *Mol Cell*
1096 70(5):842-853 e847.
1097
1098 53. Bray F*, et al.* (2018) Global cancer statistics 2018: GLOBOCAN estimates of incidence and
1099 mortality worldwide for 36 cancers in 185 countries. *CA Cancer J Clin* 68(6):394-424.
1100
1101 54. Anders CK & Carey LA (2009) Biology, metastatic patterns, and treatment of patients with triple-
1102 negative breast cancer. *Clin Breast Cancer* 9 Suppl 2:S73-81.
1103
1104 55. Cheung-Ong K, Giaever G, & Nislow C (2013) DNA-damaging agents in cancer chemotherapy:
1105 serendipity and chemical biology. *Chem Biol* 20(5):648-659.
1106
1107 56. Woods D & Turchi JJ (2013) Chemotherapy induced DNA damage response: convergence of
1108 drugs and pathways. *Cancer biology & therapy* 14(5):379-389.
1109
1110 57. Livraghi L & Garber JE (2015) PARP inhibitors in the management of breast cancer: current
1111 data and future prospects. *BMC Med* 13:188.
1112
1113 58. Giglia-Mari G, Zotter A, & Vermeulen W (2011) DNA damage response. *Cold Spring Harbor*
1114 *perspectives in biology* 3(1):a000745.
1115
1116 59. Yuan J, Adamski R, & Chen J (2010) Focus on histone variant H2AX: to be or not to be. *FEBS*
1117 *Lett* 584(17):3717-3724.
1118
1119 60. Blackford AN & Jackson SP (2017) ATM, ATR, and DNA-PK: The Trinity at the Heart of the
1120 DNA Damage Response. *Mol Cell* 66(6):801-817.
1121
1122 61. Smith J, Tho LM, Xu N, & Gillespie DA (2010) The ATM-Chk2 and ATR-Chk1 pathways in DNA
1123 damage signaling and cancer. *Advances in cancer research* 108:73-112.
1124
1125 62. Ou YH, Chung PH, Sun TP, & Shieh SY (2005) p53 C-terminal phosphorylation by CHK1 and
1126 CHK2 participates in the regulation of DNA-damage-induced C-terminal acetylation. *Mol Biol*
1127 *Cell* 16(4):1684-1695.
1128
1129 63. Thapar R (2018) Regulation of DNA Double-Strand Break Repair by Non-Coding RNAs.
1130 *Molecules* 23(11).
1131
1132 64. Liu S*, et al.* (2012) Distinct roles for DNA-PK, ATM and ATR in RPA phosphorylation and
1133 checkpoint activation in response to replication stress. *Nucleic Acids Res* 40(21):10780-10794.
1134
1135 65. Hwang J*, et al.* (2005) The time-dependent serial gene response to Zeocin treatment involves
1136 caspase-dependent apoptosis in HeLa cells. *Microbiol Immunol* 49(4):331-342.
1137
1138 66. Rudin CM & Thompson CB (2001) Transcriptional activation of short interspersed elements by
1139 DNA-damaging agents. *Genes Chromosomes Cancer* 30(1):64-71.
1140
1141 67. Hagan CR, Sheffield RF, & Rudin CM (2003) Human Alu element retrotransposition induced by
1142 genotoxic stress. *Nature genetics* 35(3):219-220.
1143

68. Britt W (2007) Virus entry into host, establishment of infection, spread in host, mechanisms of tissue damage. *Human Herpesviruses: Biology, Therapy, and Immunoprophylaxis*, eds Arvin A, Campadelli-Fiume G, Mocarski E, Moore PS, Roizman B, Whitley R, & Yamanishi KCambridge).

69. Scholz M, Doerr HW, & Cinatl J (2003) Human cytomegalovirus retinitis: pathogenicity, immune evasion and persistence. *Trends Microbiol* 11(4):171-178.

70. Port AD*, et al.* (2017) Cytomegalovirus Retinitis: A Review. *J Ocul Pharmacol Ther* 33(4):224-234.

71. Wang D & Shenk T (2005) Human cytomegalovirus virion protein complex required for epithelial and endothelial cell tropism. *Proc Natl Acad Sci U S A* 102(50):18153-18158.

72. Wang D & Shenk T (2005) Human cytomegalovirus UL131 open reading frame is required for epithelial cell tropism. *J Virol* 79(16):10330-10338.

73. Wang D, Yu QC, Schroer J, Murphy E, & Shenk T (2007) Human cytomegalovirus uses two distinct pathways to enter retinal pigmented epithelial cells. *Proc Natl Acad Sci U S A* 104(50):20037-20042.

74. Ryckman BJ*, et al.* (2008) Characterization of the human cytomegalovirus gH/gL/UL128-131 complex that mediates entry into epithelial and endothelial cells. *J Virol* 82(1):60-70.

75. Hahn G*, et al.* (2004) Human cytomegalovirus UL131-128 genes are indispensable for virus growth in endothelial cells and virus transfer to leukocytes. *J Virol* 78(18):10023-10033.

76. Gerna G*, et al.* (2005) Dendritic-cell infection by human cytomegalovirus is restricted to strains carrying functional UL131-128 genes and mediates efficient viral antigen presentation to CD8+ T cells. *J Gen Virol* 86(Pt 2):275-284.

77. Nogalski MT, Chan GC, Stevenson EV, Collins-McMillen DK, & Yurochko AD (2013) The HCMV gH/gL/UL128-131 complex triggers the specific cellular activation required for efficient viral internalization into target monocytes. *PLoS Pathog* 9(7):e1003463.

78. Waldman T, Kinzler KW, & Vogelstein B (1995) p21 is necessary for the p53-mediated G1 arrest in human cancer cells. *Cancer Res* 55(22):5187-5190.

79. Valverde M*, et al.* (2018) Hydrogen Peroxide-Induced DNA Damage and Repair through the Differentiation of Human Adipose-Derived Mesenchymal Stem Cells. *Stem Cells Int* 2018:1615497.

80. Benedict B*, et al.* (2018) Loss of p53 suppresses replication-stress-induced DNA breakage in G1/S checkpoint deficient cells. *Elife* 7.

81. Schmitt AM*, et al.* (2016) An inducible long noncoding RNA amplifies DNA damage signaling. *Nature genetics* 48(11):1370-1376.

82. Batista LF, Kaina B, Meneghini R, & Menck CF (2009) How DNA lesions are turned into powerful killing structures: insights from UV-induced apoptosis. *Mutat Res* 681(2-3):197-208.

1196 83. Roos WP & Kaina B (2013) DNA damage-induced cell death: from specific DNA lesions to the
1197 DNA damage response and apoptosis. *Cancer Lett* 332(2):237-248.
1198
1199 84. Smart DJ*, et al.* (2008) Assessment of DNA double-strand breaks and gammaH2AX induced by
1200 the topoisomerase II poisons etoposide and mitoxantrone. *Mutat Res* 641(1-2):43-47.
1201
1202 85. Shimada K*, et al.* (2013) TORC2 signaling pathway guarantees genome stability in the face of
1203 DNA strand breaks. *Mol Cell* 51(6):829-839.
1204
1205 86. Dobin A*, et al.* (2013) STAR: ultrafast universal RNA-seq aligner. *Bioinformatics* 29(1):15-21.
1206
1207 87. Subramanian A*, et al.* (2005) Gene set enrichment analysis: a knowledge-based approach for
1208 interpreting genome-wide expression profiles. *Proc Natl Acad Sci U S A* 102(43):15545-15550.
1209
1210 88. Liberzon A*, et al.* (2015) The Molecular Signatures Database (MSigDB) hallmark gene set
1211 collection. *Cell Syst* 1(6):417-425.
1212
1213 89. Kalejta RF & Shenk T (2003) Proteasome-dependent, ubiquitin-independent degradation of the
1214 Rb family of tumor suppressors by the human cytomegalovirus pp71 protein. *Proc Natl Acad Sci*
1215 *U S A* 100(6):3263-3268.
1216
1217 90. Iwahori S, Umana AC, VanDeusen HR, & Kalejta RF (2017) Human cytomegalovirus-encoded
1218 viral cyclin-dependent kinase (v-CDK) UL97 phosphorylates and inactivates the retinoblastoma
1219 protein-related p107 and p130 proteins. *J Biol Chem* 292(16):6583-6599.
1220
1221 91. Hume AJ & Kalejta RF (2009) Regulation of the retinoblastoma proteins by the human
1222 herpesviruses. *Cell Div* 4:1.
1223
1224 92. He Y, Armanious MK, Thomas MJ, & Cress WD (2000) Identification of E2F-3B, an alternative
1225 form of E2F-3 lacking a conserved N-terminal region. *Oncogene* 19(30):3422-3433.
1226
1227 93. Leone G*, et al.* (2000) Identification of a novel E2F3 product suggests a mechanism for
1228 determining specificity of repression by Rb proteins. *Mol Cell Biol* 20(10):3626-3632.
1229
1230 94. Adams MR, Sears R, Nuckolls F, Leone G, & Nevins JR (2000) Complex transcriptional
1231 regulatory mechanisms control expression of the E2F3 locus. *Mol Cell Biol* 20(10):3633-3639.
1232
1233 95. Danielian PS*, et al.* (2008) E2f3a and E2f3b make overlapping but different contributions to total
1234 E2f3 activity. *Oncogene* 27(51):6561-6570.
1235
1236 96. Chong JL*, et al.* (2009) E2f3a and E2f3b contribute to the control of cell proliferation and mouse
1237 development. *Mol Cell Biol* 29(2):414-424.
1238
1239 97. Asp P, Acosta-Alvear D, Tsikitis M, van Oevelen C, & Dynlacht BD (2009) E2f3b plays an
1240 essential role in myogenic differentiation through isoform-specific gene regulation. *Genes Dev*
1241 23(1):37-53.
1242
1243 98. Reimer D*, et al.* (2010) E2F3a is critically involved in epidermal growth factor receptor-directed
1244 proliferation in ovarian cancer. *Cancer Res* 70(11):4613-4623.
1245
1246 99. Lees JA*, et al.* (1993) The retinoblastoma protein binds to a family of E2F transcription factors.
1247 *Mol Cell Biol* 13(12):7813-7825.

100. Lukas J, Petersen BO, Holm K, Bartek J, & Helin K (1996) Deregulated expression of E2F family members induces S-phase entry and overcomes p16INK4A-mediated growth suppression. *Mol Cell Biol* 16(3):1047-1057.

101. Baker SJ, Markowitz S, Fearon ER, Willson JK, & Vogelstein B (1990) Suppression of human colorectal carcinoma cell growth by wild-type p53. *Science* 249(4971):912-915.

102. Iglesias-Ara A & Zubiaga AM (2016) The stress of coping with E2F loss. *Mol Cell Oncol* 3(1):e1038423.

103. Liao CC, Tsai CY, Chang WC, Lee WH, & Wang JM (2010) RB.E2F1 complex mediates DNA damage responses through transcriptional regulation of ZBRK1. *J Biol Chem* 285(43):33134-33143.

104. Shamma A*, et al.* (2009) Rb Regulates DNA damage response and cellular senescence through E2F-dependent suppression of N-ras isoprenylation. *Cancer Cell* 15(4):255-269.

105. Falck J, Coates J, & Jackson SP (2005) Conserved modes of recruitment of ATM, ATR and DNA-PKcs to sites of DNA damage. *Nature* 434(7033):605-611.

106. Ziv Y*, et al.* (1989) Cellular and molecular characteristics of an immortalized ataxia-telangiectasia (group AB) cell line. *Cancer Res* 49(9):2495-2501.

107. Ziv Y*, et al.* (1997) Recombinant ATM protein complements the cellular A-T phenotype. *Oncogene* 15(2):159-167.

108. Hickson I*, et al.* (2004) Identification and characterization of a novel and specific inhibitor of the ataxia-telangiectasia mutated kinase ATM. *Cancer Res* 64(24):9152-9159.

109. Greene J*, et al.* (2017) The novel ATM inhibitor (AZ31) enhances antitumor activity in patient derived xenografts that are resistant to irinotecan monotherapy. *Oncotarget* 8(67):110904-110913.

110. Li Y & Yang DQ (2010) The ATM inhibitor KU-55933 suppresses cell proliferation and induces apoptosis by blocking Akt in cancer cells with overactivated Akt. *Mol Cancer Ther* 9(1):113-125.

111. Castillo JP*, et al.* (2005) Human cytomegalovirus IE1-72 activates ataxia telangiectasia mutated kinase and a p53/p21-mediated growth arrest response. *J Virol* 79(17):11467-11475.

112. Song YJ & Stinski MF (2005) Inhibition of cell division by the human cytomegalovirus IE86 protein: role of the p53 pathway or cyclin-dependent kinase 1/cyclin B1. *J Virol* 79(4):2597-2603.

113. Tanaka K*, et al.* (1999) Effects of human cytomegalovirus immediate-early proteins on p53-mediated apoptosis in coronary artery smooth muscle cells. *Circulation* 99(13):1656-1659.

114. Hwang ES*, et al.* (2009) Human cytomegalovirus IE1-72 protein interacts with p53 and inhibits p53-dependent transactivation by a mechanism different from that of IE2-86 protein. *J Virol* 83(23):12388-12398.

1299 115. Li Y*, et al.* (2018) Expression patterns of E2F transcription factors and their potential prognostic
1300 roles in breast cancer. *Oncol Lett* 15(6):9216-9230.
1301
1302 116. Renwick A*, et al.* (2006) ATM mutations that cause ataxia-telangiectasia are breast cancer
1303 susceptibility alleles. *Nature genetics* 38(8):873-875.
1304
1305 117. Thompson D*, et al.* (2005) Cancer risks and mortality in heterozygous ATM mutation carriers. *J*
1306 *Natl Cancer Inst* 97(11):813-822.
1307
1308 118. Dai X, Cheng H, Bai Z, & Li J (2017) Breast Cancer Cell Line Classification and Its Relevance
1309 with Breast Tumor Subtyping. *J Cancer* 8(16):3131-3141.
1310
1311 119. Justus CR, Leffler N, Ruiz-Echevarria M, & Yang LV (2014) In vitro cell migration and invasion
1312 assays. *J Vis Exp* (88).
1313
1314 120. Liu YL*, et al.* (2019) Assessing metastatic potential of breast cancer cells based on EGFR
1315 dynamics. *Sci Rep* 9(1):3395.
1316
1317 121. Taubenberger AV, Quent VM, Thibaudeau L, Clements JA, & Hutmacher DW (2013)
1318 Delineating breast cancer cell interactions with engineered bone microenvironments. *Journal of*
1319 *bone and mineral research : the official journal of the American Society for Bone and Mineral*
1320 *Research* 28(6):1399-1411.
1321
1322 122. Liang CC, Park AY, & Guan JL (2007) In vitro scratch assay: a convenient and inexpensive
1323 method for analysis of cell migration in vitro. *Nature protocols* 2(2):329-333.
1324
1325 123. Marceau N, Goyette R, Deschenes J, & Valet JP (1980) Morphological differences between
1326 epithelial and fibroblast cells in rat liver cultures, and the roles of cell surface fibronectin and
1327 cytoskeletal element organization in cell shape. *Ann N Y Acad Sci* 349:138-152.
1328
1329 124. Wilkes MC, Murphy SJ, Garamszegi N, & Leof EB (2003) Cell-type-specific activation of PAK2
1330 by transforming growth factor beta independent of Smad2 and Smad3. *Mol Cell Biol*
1331 23(23):8878-8889.
1332
1333 125. Mallinjoud P*, et al.* (2014) Endothelial, epithelial, and fibroblast cells exhibit specific splicing
1334 programs independently of their tissue of origin. *Genome Res* 24(3):511-521.
1335
1336 126. Oberstein A & Shenk T (2017) Cellular responses to human cytomegalovirus infection: Induction
1337 of a mesenchymal-to-epithelial transition (MET) phenotype. *Proc Natl Acad Sci U S A*.
1338
1339 127. Dargan DJ*, et al.* (2010) Sequential mutations associated with adaptation of human
1340 cytomegalovirus to growth in cell culture. *J Gen Virol* 91(Pt 6):1535-1546.
1341
1342 128. Stanton RJ*, et al.* (2010) Reconstruction of the complete human cytomegalovirus genome in a
1343 BAC reveals RL13 to be a potent inhibitor of replication. *J Clin Invest* 120(9):3191-3208.
1344
1345 129. Li G, Nguyen CC, Ryckman BJ, Britt WJ, & Kamil JP (2015) A viral regulator of glycoprotein
1346 complexes contributes to human cytomegalovirus cell tropism. *Proc Natl Acad Sci U S A*
1347 112(14):4471-4476.
1348
1349 130. Tomasec P*, et al.* (2005) Downregulation of natural killer cell-activating ligand CD155 by human
1350 cytomegalovirus UL141. *Nat Immunol* 6(2):181-188.

131. Wills MR, *et al.* (2005) Human cytomegalovirus encodes an MHC class I-like molecule (UL142) that functions to inhibit NK cell lysis. *J Immunol* 175(11):7457-7465.

132. E X, *et al.* (2011) An E2F1-mediated DNA damage response contributes to the replication of human cytomegalovirus. *PLoS Pathog* 7(5):e1001342.

133. Halaby MJ, Hibma JC, He J, & Yang DQ (2008) ATM protein kinase mediates full activation of Akt and regulates glucose transporter 4 translocation by insulin in muscle cells. *Cell Signal* 20(8):1555-1563.

134. Miyamoto S (2011) Nuclear initiated NF-kappaB signaling: NEMO and ATM take center stage. *Cell Res* 21(1):116-130.

135. Yurochko AD, Kowalik TF, Huong SM, & Huang ES (1995) Human cytomegalovirus upregulates NF-kappa B activity by transactivating the NF-kappa B p105/p50 and p65 promoters. *J Virol* 69(9):5391-5400.

136. Caposio P, Dreano M, Garotta G, Gribaudo G, & Landolfo S (2004) Human cytomegalovirus stimulates cellular IKK2 activity and requires the enzyme for productive replication. *J Virol* 78(6):3190-3195.

137. DeMeritt IB, Milford LE, & Yurochko AD (2004) Activation of the NF-kappaB pathway in human cytomegalovirus-infected cells is necessary for efficient transactivation of the major immediate-early promoter. *J Virol* 78(9):4498-4507.

138. DeMeritt IB, Podduturi JP, Tilley AM, Nogalski MT, & Yurochko AD (2006) Prolonged activation of NF-kappaB by human cytomegalovirus promotes efficient viral replication and late gene expression. *Virology* 346(1):15-31.

139. Browne EP & Shenk T (2003) Human cytomegalovirus UL83-coded pp65 virion protein inhibits antiviral gene expression in infected cells. *Proc Natl Acad Sci U S A* 100(20):11439-11444.

140. Jarvis MA, *et al.* (2006) Human cytomegalovirus attenuates interleukin-1beta and tumor necrosis factor alpha proinflammatory signaling by inhibition of NF-kappaB activation. *J Virol* 80(11):5588-5598.

141. Landini MP (1984) Early enhanced glucose uptake in human cytomegalovirus-infected cells. *J Gen Virol* 65 (Pt 7):1229-1232.

142. Yu Y, Clippinger AJ, & Alwine JC (2011) Viral effects on metabolism: changes in glucose and glutamine utilization during human cytomegalovirus infection. *Trends Microbiol* 19(7):360-367.

143. Yu Y, Maguire TG, & Alwine JC (2011) Human cytomegalovirus activates glucose transporter 4 expression to increase glucose uptake during infection. *J Virol* 85(4):1573-1580.

144. Furukawa T, Sakuma S, & Plotkin SA (1976) Human cytomegalovirus infection of WI-38 cells stimulates mitochondrial DNA synthesis. *Nature* 262(5567):414-416.

145. McCormick AL, Smith VL, Chow D, & Mocarski ES (2003) Disruption of mitochondrial networks by the human cytomegalovirus UL37 gene product viral mitochondrion-localized inhibitor of apoptosis. *J Virol* 77(1):631-641.

146. Karniely S, *et al.* (2016) Human Cytomegalovirus Infection Upregulates the Mitochondrial Transcription and Translation Machineries. *mBio* 7(2):e00029.

147. Hay N (2016) Reprogramming glucose metabolism in cancer: can it be exploited for cancer therapy? *Nat Rev Cancer* 16(10):635-649.

148. Bose S & Le A (2018) Glucose Metabolism in Cancer. *Adv Exp Med Biol* 1063:3-12.

149. Xia Y, Shen S, & Verma IM (2014) NF-kappaB, an active player in human cancers. *Cancer Immunol Res* 2(9):823-830.

150. Taniguchi K & Karin M (2018) NF-kappaB, inflammation, immunity and cancer: coming of age. *Nat Rev Immunol* 18(5):309-324.

151. Chang JY, Yi HS, Kim HW, & Shong M (2017) Dysregulation of mitophagy in carcinogenesis and tumor progression. *Biochim Biophys Acta Bioenerg* 1858(8):633-640.

152. Vara-Perez M, Felipe-Abrio B, & Agostinis P (2019) Mitophagy in Cancer: A Tale of Adaptation. *Cells* 8(5).

153. Paulson QX, McArthur MJ, & Johnson DG (2006) E2F3a stimulates proliferation, p53-independent apoptosis and carcinogenesis in a transgenic mouse model. *Cell Cycle* 5(2):184-190.

154. Cremona CA & Behrens A (2014) ATM signalling and cancer. *Oncogene* 33(26):3351-3360.

155. Kondratova VN, Botezatu IV, Shelepov VP, & Likhtenshtein AV (2014) [Transcripts of satellite DNA in blood plasma: probable markers of tumor growth]. *Mol Biol (Mosk)* 48(6):999-1007.

156. Kishikawa T, *et al.* (2016) Quantitation of circulating satellite RNAs in pancreatic cancer patients. *JCI Insight* 1(8):e86646.

157. Pandey JP, *et al.* (2016) Humoral Immunity to Cytomegalovirus Glycoprotein B in Patients With Breast Cancer and Matched Controls: Contribution of Immunoglobulin gamma, kappa, and Fcgamma Receptor Genes. *J Infect Dis* 213(4):611-617.

158. Naucler CS, Geisler J, & Vetvik K (2019) The emerging role of human cytomegalovirus infection in human carcinogenesis: a review of current evidence and potential therapeutic implications. *Oncotarget* 10(42):4333-4347.

159. Costa H, *et al.* (2019) Human cytomegalovirus infection is correlated with enhanced cyclooxygenase-2 and 5-lipoxygenase protein expression in breast cancer. *J Cancer Res Clin Oncol* 145(8):2083-2095.

160. Pasquereau S, *et al.* (2017) Cytomegalovirus, Macrophages and Breast Cancer. *The open virology journal* 11:15-27.

161. Neve RM, *et al.* (2006) A collection of breast cancer cell lines for the study of functionally distinct cancer subtypes. *Cancer Cell* 10(6):515-527.

162. Murphy E*, et al.* (2003) Coding potential of laboratory and clinical strains of human cytomegalovirus. *Proc Natl Acad Sci U S A* 100(25):14976-14981.

163. Wu K, Oberstein A, Wang W, & Shenk T (2018) Role of PDGF receptor-alpha during human cytomegalovirus entry into fibroblasts. *Proc Natl Acad Sci U S A* 115(42):E9889-E9898.

164. Reed LJ & Muench H (1938) A simple method of estimating fifty percent endpoints. *The American Journal of Hygiene* 27:493-497.

165. Afgan E*, et al.* (2018) The Galaxy platform for accessible, reproducible and collaborative biomedical analyses: 2018 update. *Nucleic Acids Res* 46(W1):W537-W544.

166. Liao Y, Smyth GK, & Shi W (2014) featureCounts: an efficient general purpose program for assigning sequence reads to genomic features. *Bioinformatics* 30(7):923-930.

167. Love MI, Huber W, & Anders S (2014) Moderated estimation of fold change and dispersion for RNA-seq data with DESeq2. *Genome Biol* 15(12):550.

168. Thorvaldsdottir H, Robinson JT, & Mesirov JP (2013) Integrative Genomics Viewer (IGV): high-performance genomics data visualization and exploration. *Brief Bioinform* 14(2):178-192.

169. Heberle H, Meirelles GV, da Silva FR, Telles GP, & Minghim R (2015) InteractiVenn: a web-based tool for the analysis of sets through Venn diagrams. *BMC Bioinformatics* 16:169.

170. Livak KJ & Schmittgen TD (2001) Analysis of relative gene expression data using real-time quantitative PCR and the 2(-Delta Delta C(T)) Method. *Methods* 25(4):402-408.

171. Zhu H, Shen Y, & Shenk T (1995) Human cytomegalovirus IE1 and IE2 proteins block apoptosis. *J Virol* 69(12):7960-7970.

172. Cuevas-Bennett C & Shenk T (2008) Dynamic histone H3 acetylation and methylation at human cytomegalovirus promoters during replication in fibroblasts. *J Virol* 82(19):9525-9536.

173. Lu M & Shenk T (1999) Human cytomegalovirus UL69 protein induces cells to accumulate in G1 phase of the cell cycle. *J Virol* 73(1):676-683.

174. Hwang J & Kalejta RF (2007) Proteasome-dependent, ubiquitin-independent degradation of Daxx by the viral pp71 protein in human cytomegalovirus-infected cells. *Virology* 367(2):334-338.

175. Silva MC, Yu QC, Enquist L, & Shenk T (2003) Human cytomegalovirus UL99-encoded pp28 is required for the cytoplasmic envelopment of tegument-associated capsids. *J Virol* 77(19):10594-10605.

176. Rajapakse D, Peterson K, Mishra S, & Wistow G (2017) Serum starvation of ARPE-19 changes the cellular distribution of cholesterol and Fibulin3 in patterns reminiscent of age-related macular degeneration. *Exp Cell Res* 361(2):333-341.

177. Upadhyay S, Vaish S, & Dhiman M (2019) Hydrogen peroxide-induced oxidative stress and its impact on innate immune responses in lung carcinoma A549 cells. *Mol Cell Biochem* 450(1-2):135-147.

178. Nakajima S, *et al.* (2004) UV light-induced DNA damage and tolerance for the survival of nucleotide excision repair-deficient human cells. *J Biol Chem* 279(45):46674-46677.

179. Rasband WS (1997-2010) ImageJ (U.S. National Institutes of Health, Bethesda, Maryland, USA).

1543 **Figure legends**

1544

1545 **Figure 1. HSATII KD has strong effect on HCMV infection in epithelial cells. (A)** RNA samples
1546 were collected at 24 hpi from ARPE-19 cells transfected with NT-LNA or HSATII-LNAs 24 h before
1547 HCMV (TB40/E-GFP-epi) infection at 1 TCID50/cell. RT-qPCR was performed using HSATII-specific
1548 primers. GAPDH was used as an internal control. Data are presented as a fold change mean ± SD.
1549 n=3. **(B)** Protein samples were collected at indicated times from ARPE-19 cells transfected with NT-
1550 LNA or HSATII-LNAs 24 h before HCMV (TB40/E-GFP-epi) infection at 1 $TCID_{50}$/cell. Protein levels
1551 were analyzed by the western blot technique using antibodies specific to IE1, IE2, pUL26, pUL44,
1552 pUL69, pp71 and pp28. Actin was used as a loading control. **(C)** Total DNA was collected at indicated
1553 times from ARPE-19 cells transfected with NT-LNA or HSATII-LNAs 24 h before HCMV (TB40/E-GFP-
1554 epi) infection at 1 TCID50/cell. vDNA and cellular DNA copy numbers were determined. Data are
1555 presented as a fold change mean ± SD of the relative vDNA to cellular DNA ratio. n=3 **(D)** Media
1556 samples were collected at indicated times from ARPE-19 cells transfected with NT-LNA or HSATII-
1557 LNAs 24 h before HCMV (TB40/E-GFP-epi) infection at 1 $TCID_{50}$/cell. TCID50 ml^{-1} values were
1558 determined**. (E)** Intracellular and extracellular virions were collected at indicated times from ARPE-19
1559 cells transfected with either NT-LNA, HSATII-LNA#1, HSATII-LNA#2 or both HSATII-LNAs 24 h before
1560 HCMV (TB40/E-GFP-epi) infection at 1 $TCID_{50}$/cell. TCID50 ml^{-1} values were determined**.** Data are
1561 presented as a mean ± SD. *n*=3. ****P*<0.001, *****P*<0.0001 by the unpaired, two-tailed *t*-test.

1562

1563 **Figure 2. DNA damage response regulates HSATII expression. (A)** ARPE-19 cells were exposed to
1564 UV-irradiation (50 J/m^2), 100 nM of H_2O_2 or serum withdrawal. RNA samples were collected at 24 hpt.
1565 RT-qPCR was performed using specific primers to HSATII, CDKN1A or DINO transcripts. GAPDH was
1566 used as an internal control. Data are presented as a fold change mean ± SD. n =3. **P*<0.05, ***P*<0.01,
1567 ****P*<0.001 by the unpaired, two-tailed *t*-test. **(B and C)** ARPE-19 cells were treated with increasing
1568 concentrations of zeocin or etoposide. H_2O or DMSO, respectively, were used as solvent controls. RNA
1569 samples were collected at 24 hpt. RT-qPCR was performed using specific primers to HSATII, CDKN1A
1570 or DINO transcripts. GAPDH was used as an internal control. Data are presented as a fold change
1571 mean ± SD. n =3. Insert: At 24 hpt, cell viability was assessed at each indicated drug concentrations.
1572 Data is presented as % viable cells, were averaged from at least three independent experiments and
1573 are presented as mean (SD). **(D and E)** ARPE-19 cells were treated with 200 μg/mL of zeocin, 200 μM
1574 of etoposide and either with H_2O or DMSO, respectively, as solvent controls. RNA samples were
1575 collected at indicated times. RT-qPCR was performed using specific primers for HSATII, CDKN1A or
1576 DINO transcripts. GAPDH was used as an internal control. Data are presented as a fold change mean
1577 ± SD. n =3. **(F)** ARPE-19 cells were mock- or HCMV (TB40/E-GFP-epi)-infected at 1 $TCID_{50}$/cell, or

1578 treated with 200 μg/mL of zeocin or H_2O as a solvent control. After 24 h, RNA samples were collected,
1579 RNA was isolated and analyzed using RNA-seq. Reads were mapped to human genome assembly
1580 hg19 and read coverage tracks at the HSATII locus on chromosome 16 were visualized using IGV.
1581
1582 **Figure 3. Zeocin partially mimics transcriptional effect of HCMV.** ARPE-19 cells were mock- or
1583 HCMV (TB40/E-GFP-epi)-infected at 1 $TCID_{50}$/cell, or treated with 200 μg/mL of zeocin or H_2O as a
1584 solvent control. After 24 h, RNA samples were collected, RNA was isolated and analyzed using RNA-
1585 seq. **(A)** Venn diagram shows differentially expressed genes ($q<0.05$) either in HCMV-infected or
1586 zeocin-treated cells vs. respective controls. **(B)** GSEA was performed on the list of common genes
1587 differentially expressed in both HCMV-infected and zeocin-treated cells using the hallmark gene set of
1588 MSigDB. Identified specific gene set names are categorized based on increasing *p*-value and FDR q-
1589 value.
1590
1591 **Figure 4. Transcription factor E2F3a regulates HSATII expression. (A)** ARPE-19 cells were
1592 transfected with E2F1, E2F2, E2F3, E2F4, E2F5 siRNAs or NT siRNA as a control. After 24 h, cells
1593 were infected with TB40/E-GFP-epi at 1 TCID50 per cell. RNA samples were collected at 24 hpi. RT-
1594 qPCR was performed using specific primers to HSATII, E2F1, E2F2, E2F3, E2F4 or E2F5 transcripts.
1595 GAPDH was used as an internal control. Data are presented as a fold change mean ± SD. n =3. **(B)**
1596 Tetracycline-inducible IE1 and IE2 ARPE-19 cells were transfected with E2F3 siRNA or NT siRNA as a
1597 control. After 48 h, cells were treated with doxycycline. RNA samples were collected at 24 hpt. RT-
1598 qPCR was performed using specific primers to HSATII, E2F3, as well as viral UL122 and UL123
1599 transcripts. GAPDH was used as an internal control. Data are presented as a fold change mean ± SD.
1600 n =3. **(C)** ARPE-19 cells were transfected with E2F1-, E2F2-, E2F3a- or E2F3b-expressing plasmids.
1601 After 72 h, RNA samples were collected. RT-qPCR was performed using specific primers to HSATII,
1602 E2F1, E2F2, E2F3a or E2F3b transcripts. GAPDH was used as an internal control. Data are presented
1603 as a fold change mean ± SD. n =3. **(D)** ARPE-19 cells were mock- or HCMV infected (TB40/E-GFP-epi)
1604 at 3 TCID50 per cell, treated with 200 μg/mL of Zeocin or 200 μM of etoposide and either with H_2O or
1605 DMSO, respectively, as solvent controls. RNA samples were collected at 24 hpt. RT-qPCR was
1606 performed using HSATII RNA specific primers. GAPDH was used as an internal control. Data are
1607 presented as a fold change mean ± SD. n =3. **(E)** Tetracycline-inducible ARPE-19 cells were either
1608 treated with doxycycline or were infected with HCMV (TB40/E-GFP-epi) at 3 TCID50 /cell for 24, 48, 72,
1609 or 96 h. Protein samples were collected at indicated times. Protein levels were analyzed by western
1610 blotting using anti-IE1, anti-IE2 or anti-E2F3 antibodies. Actin was used as a loading control. **(F)** ARPE-
1611 19 cells were transfected with E2F3 siRNA or NT siRNA as a control. After 24 h, cells were infected
1612 with TB40/E-GFP-epi at 1 TCID50 per cell. RNA samples were collected at 24 hpi. RT-qPCR was

1613 performed using specific primers to UL123, UL37x1, UL26, UL54, UL82 or UL99 transcripts. GAPDH
1614 was used as an internal control. Data are presented as a fold change mean ± SD. n =3. **(G)** ARPE-19
1615 cells were treated with 200 μg/mL of zeocin. After 24 h, cells were infected with TB40/E-GFP-epi at 1
1616 TCID50 per cell. Media were collected at 96 hpi and virus yields were determined. Results are
1617 presented as an average PFU/mL ± SD. n =3. *P<0.05, **P<0.01, ***P<0.001, ****P<0.0001 by the
1618 unpaired, two-tailed *t*-test.
1619
1620 **Figure 5. ATM-based DNA damage response regulates HSATII expression. (A and B)** ARPE-19
1621 cells were mock- or HCMV-infected with HCMV (TB40/E-GFP-epi) at 3 TCID50 /cell or treated with 200
1622 μg/mL of zeocin. Cells were stained for γ-H2AX and nuclei were counterstained with the Hoechst stain.
1623 Cells were visualized (20X magnification) **(A)** and % of γ-H2AX-positive cells was calculated **(B)** using
1624 Operetta high-content imaging and analysis system. Scale bars: 100 µm. **(C and D)** ARPE-19 cells
1625 were transfected with ATM, ATR or DNA-PK siRNAs or NT siRNA as a control. After 24 h, cells were
1626 infected with TB40/E-GFP-epi at 1 TCID50 per cell (A) or 100 μg/mL of zeocin (B). RNA samples were
1627 collected 24 h later. RT-qPCR was performed using specific primers to HSATII, ATM, ATR or DNA-PK
1628 transcripts. GAPDH was used as an internal control. Data are presented as a fold change mean ± SD.
1629 n =3. **(E)** A-T(+) and A-T(-) cells were infected with TB40/E-GFP-epi at 1 TCID50 per cell, 200 μg/mL of
1630 zeocin or 200 μM of etoposide. RNA samples were collected 24 h later. RT-qPCR was performed using
1631 specific primers to HSATII, CDKN1A or DINO transcripts. GAPDH was used as an internal control.
1632 Data are presented as a fold change mean ± SD. n =3. **(F)** ARPE-19 cells were treated with DMSO, 20
1633 μM of either Ku-55933 or AZ31 for 2 h before zeocin was added at the concentration of 100 μg/mL.
1634 RNA samples were collected 24 hpt. RT-qPCR was performed using specific primers to HSATII,
1635 CDKN1A or DINO transcripts. GAPDH was used as an internal control. Data are presented as a fold
1636 change mean ± SD. n =3. (G) ARPE-19 cells were treated with various concentrations of Ku-55933 or
1637 AZ31. At 24 hpt, cell viability was assessed. Data is presented as % viable cells, were averaged from at
1638 least three independent experiments and are presented as mean (SD). *P<0.05, **P<0.01, ***P<0.001,
1639 ****P<0.0001 by the unpaired, two-tailed *t*-test.
1640
1641 **Figure 6. HSATII expression is induced *via* Chk1/2- and p53-independent pathway**. **(A)** ARPE-19
1642 cells were transfected with CHEK1, CHEK2 siRNAs or NT siRNA as a control. After 24 h, cells were
1643 infected with TB40/E-GFP-epi at 1 TCID50 per cell or 200 μg/mL of zeocin. RNA samples were
1644 collected 24 h later. RT-qPCR was performed using specific primers to HSATII, CHEK1 or CHEK2
1645 transcripts. GAPDH was used as an internal control. Data are presented as a fold change mean ± SD.
1646 n =3. **(B and C)** ARPE-19 cells were infected with TB40/E-GFP-epi at 3 TCID50 per cell or 200 μg/mL
1647 of zeocin. RNA samples were collected 24 and 96 h later. RT-qPCR was performed using specific

1648 primers to HSATII, CDKN1A or DINO transcripts. GAPDH was used as an internal control. Data are
1649 presented as a fold change mean ± SD. n =3. **(D and E)** ARPE-19 cells were transfected with TP53
1650 siRNAs or NT siRNA as a control. After 24 h, cells were infected with TB40/E-GFP-epi at 1 TCID50 per
1651 cell or 200 μg/mL of zeocin. RNA samples were collected 24 h later. RT-qPCR was performed using
1652 specific primers to HSATII, TP53, CDKN1A or DINO transcripts. GAPDH was used as an internal
1653 control. Data are presented as a fold change mean ± SD. n =3. *P<0.05, **P<0.01, ***P<0.001,
1654 ****P<0.0001 by the unpaired, two-tailed *t*-test.
1655
1656 **Figure 7. DNA damage-induced HSATII RNA enhances motility and proliferation of breast cancer**
1657 **cells. (A)** Indicated cell lines, ordered according to the p53 status, were grown to ~80% confluency and
1658 RNA samples were collected. RT-qPCR was performed using specific primers to HSATII RNA. GAPDH
1659 was used as an internal control. Data are presented as a fold change mean ± SD. n =3. **(B)** MCF-7,
1660 MCF-10A, MDA-MB-361 and SUM1315MO2 cells were treated with 200 μg/mL of Zeocin. RNA
1661 samples were collected at 24 and 96 hpt. RT-qPCR was performed using specific primers to HSATII
1662 RNA. GAPDH was used as an internal control. Data are presented as a fold change mean ± SD. n =3.
1663 **(C)** ARPE-1, MCF-7 and SUM315MO2 cells were treated with 200 μg/mL of Zeocin for 24 h. Cells were
1664 transferred onto transwell inserts. After 24 hpt, migrated cells were washed, fixed and nuclei stained.
1665 The graph presents a number of cells (with their indicated means) migrated through a transwell per
1666 FOV from biological replicates. *n*=9-12. **(D)** MDA-MB-231, BT-549 and SUM1315MO2 cells were
1667 transfected with NT-LNA or HSATII-LNAs. After 48 hpi, equal number of cells was transferred onto
1668 transwell inserts. 24 h later, migrated cells were washed, fixed and nuclei stained. The graph presents
1669 a number of cells (with their indicated means) migrated through a transwell per FOV from biological
1670 replicates. *n*=12. **(E)** MDA-MB-231, BT-549 and SUM1315MO2 cells were transfected with NT-LNA or
1671 HSATII-LNAs. After 48 hpi, wounds were created and their closure was monitored at indicated times.
1672 Data from biological replicates are presented as a percent of remaining wound width mean ± SD. n=6.
1673 **(F)** MDA-MB-231, BT-549 and SUM1315MO2 cells were transfected with NT-LNA or HSATII-LNAs.
1674 After 48 hpt, equal number of cells were seeded and cell proliferation was monitored using a
1675 colorimetric CellTiter 96 AQueous One Solution Cell Proliferation Assay at the indicated times. Cell
1676 proliferation is presented as an increase in a measured absorbance (AU – arbitrary units). n=3.
1677 *P<0.05, **P<0.01, ***P<0.001, ****P<0.0001 by the unpaired, two-tailed *t*-test.
1678

Figures

Figure 1.

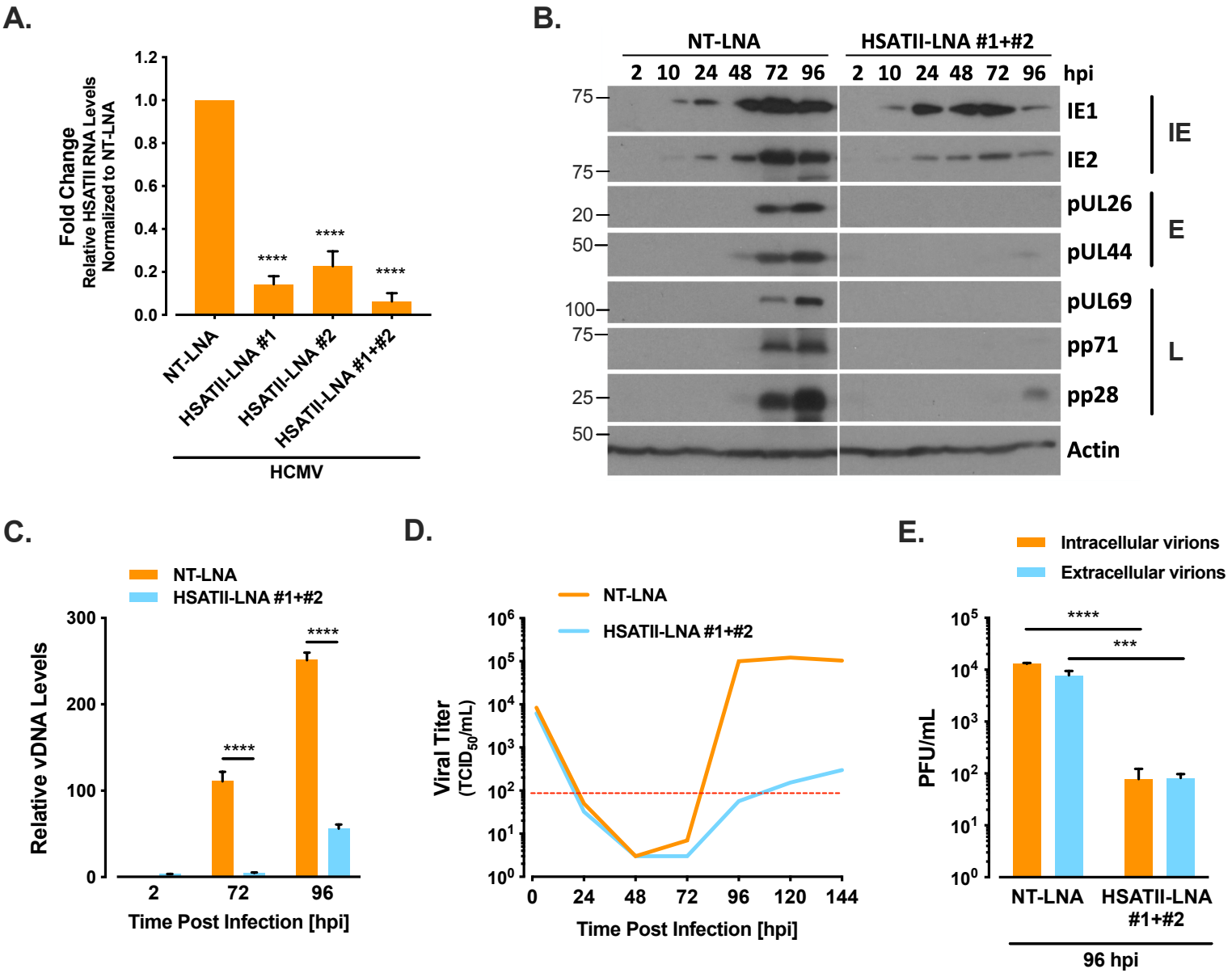

Figure 2.

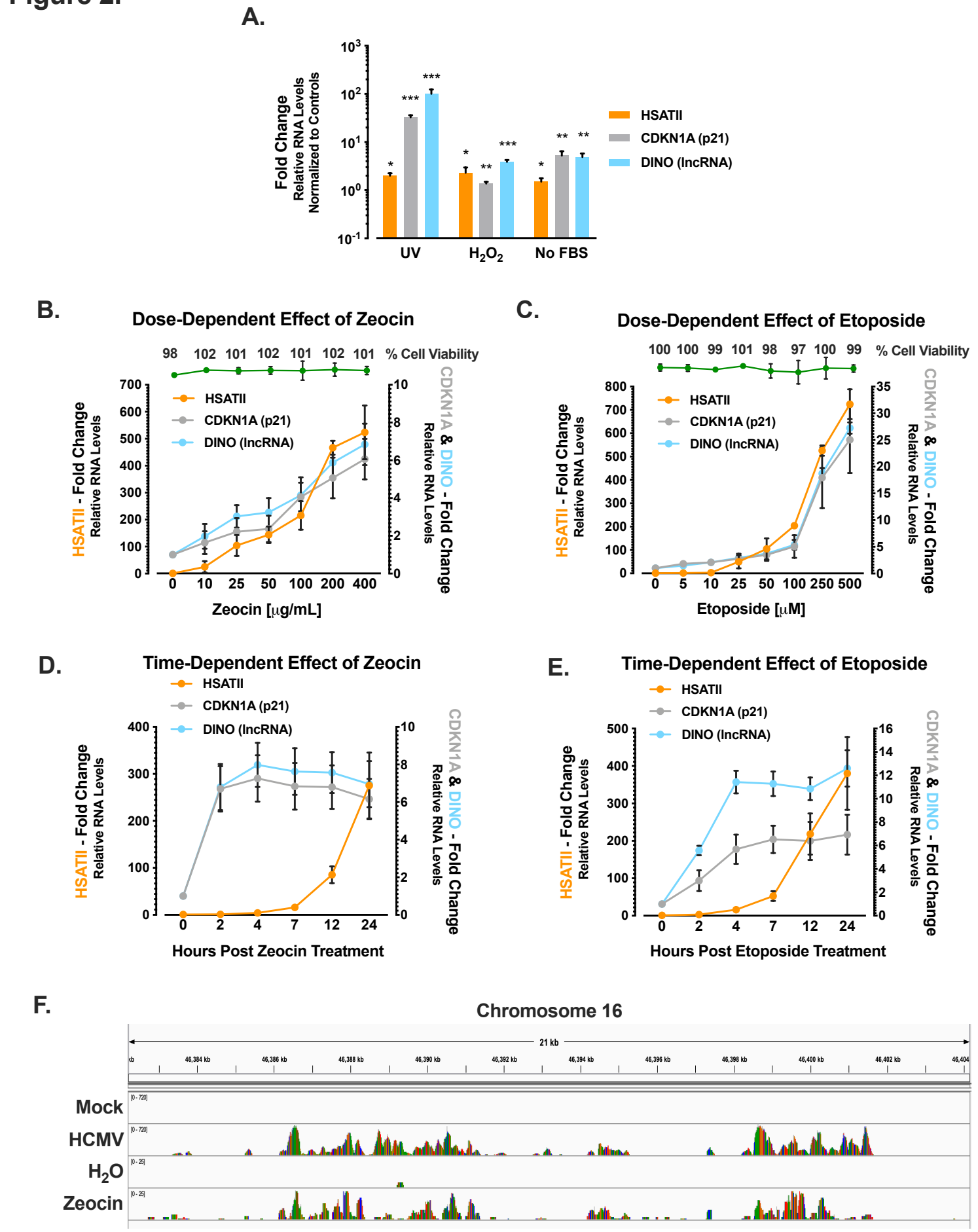
A.
Fold Change
Relative RNA Levels
Normalized to Controls
HSATII
CDKN1A (p21)
DINO (lncRNA)
UV
H2O2
No FBS
B.
Dose-Dependent Effect of Zeocin
% Cell Viability
HSATII - Fold Change
Relative RNA Levels
CDKN1A & DINO - Fold Change
Relative RNA Levels
Zeocin [μg/mL]
C.
Dose-Dependent Effect of Etoposide
Etoposide [μM]
D.
Time-Dependent Effect of Zeocin
Hours Post Zeocin Treatment
E.
Time-Dependent Effect of Etoposide
Hours Post Etoposide Treatment
F.
Chromosome 16
21 kb
Mock
HCMV
H2O
Zeocin

Figure 3.

A.

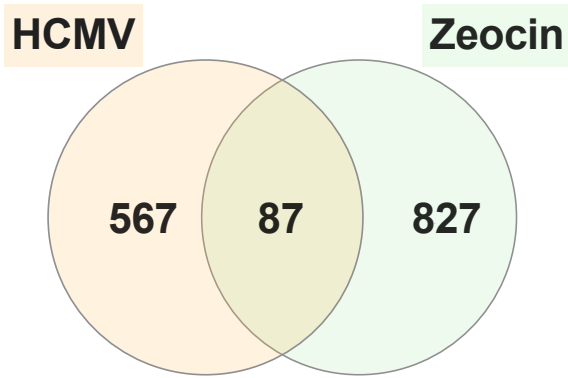

B.

Gene Set Name [# Genes (K)]	Description	p-value	FDR q-value
HALLMARK_E2F_TARGETS [200]	Genes encoding cell cycle related targets of E2F transcription factors.	$2.64\ e^{-17}$	$1.32\ e^{-15}$
HALLMARK_G2M_CHECKPOINT [200]	Genes involved in the G2/M checkpoint, as in progression through the cell division cycle.	$3.31\ e^{-11}$	$8.26\ e^{-10}$
HALLMARK_EPITHELIAL_MESENCHYMAL_TRANSITION [200]	Genes defining epithelial-mesenchymal transition, as in wound healing, fibrosis and metastasis.	$9.52\ e^{-5}$	$1.59\ e^{-3}$
HALLMARK_INTERFERON_GAMMA_RESPONSE [200]	Genes up-regulated in response to IFNG [GeneID=3458].	$1.13\ e^{-3}$	$1.13\ e^{-2}$
HALLMARK_MTORC1_SIGNALING [200]	Genes up-regulated through activation of mTORC1 complex.	$1.13\ e^{-3}$	$1.13\ e^{-2}$
HALLMARK_HEDGEHOG_SIGNALING [36]	Genes up-regulated by activation of hedgehog signaling.	$3.04\ e^{-3}$	$2.53\ e^{-2}$
HALLMARK_DNA_REPAIR [150]	Genes involved in DNA repair.	$4.87\ e^{-3}$	$3.48\ e^{-2}$
HALLMARK_APOPTOSIS [161]	Genes mediating programmed cell death (apoptosis) by activation of caspases.	$5.92\ e^{-3}$	$3.7\ e^{-2}$

Figure 4.

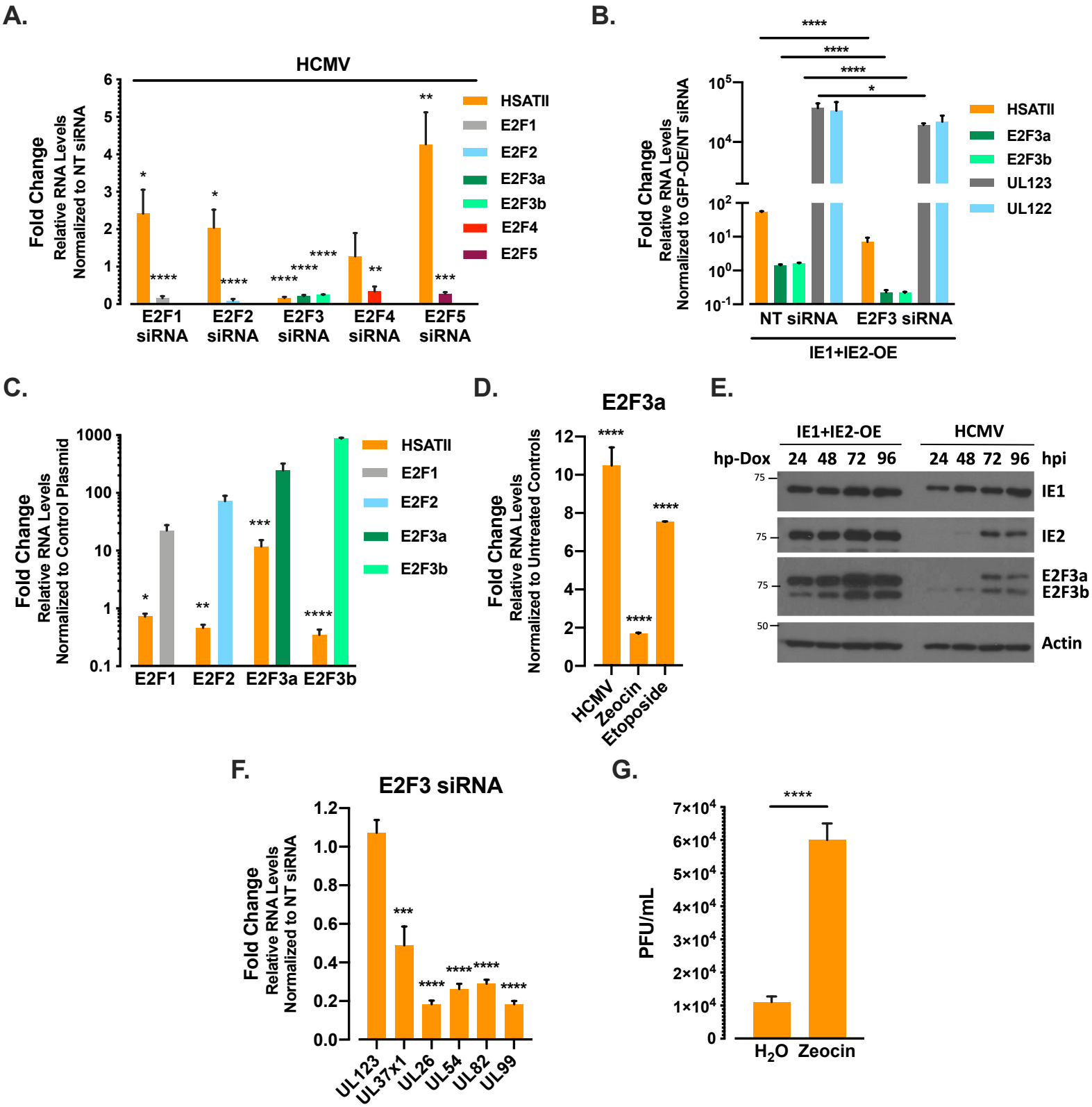
A.
HCMV
Fold Change
Relative RNA Levels
Normalized to NT siRNA
HSATII
E2F1
E2F2
E2F3a
E2F3b
E2F4
E2F5
E2F1 siRNA
E2F2 siRNA
E2F3 siRNA
E2F4 siRNA
E2F5 siRNA
B.
Fold Change
Relative RNA Levels
Normalized to GFP-OE/NT siRNA
HSATII
E2F3a
E2F3b
UL123
UL122
NT siRNA
E2F3 siRNA
IE1+IE2-OE
C.
Fold Change
Relative RNA Levels
Normalized to Control Plasmid
HSATII
E2F1
E2F2
E2F3a
E2F3b
D.
E2F3a
Fold Change
Relative RNA Levels
Normalized to Untreated Controls
HCMV
Zeocin
Etoposide
E.
IE1+IE2-OE
HCMV
hp-Dox
24 48 72 96
24 48 72 96
hpi
IE1
IE2
E2F3a
E2F3b
Actin
F.
E2F3 siRNA
Fold Change
Relative RNA Levels
Normalized to NT siRNA
UL123
UL37x1
UL26
UL54
UL82
UL99
G.
PFU/mL
H2O
Zeocin

Figure 5.

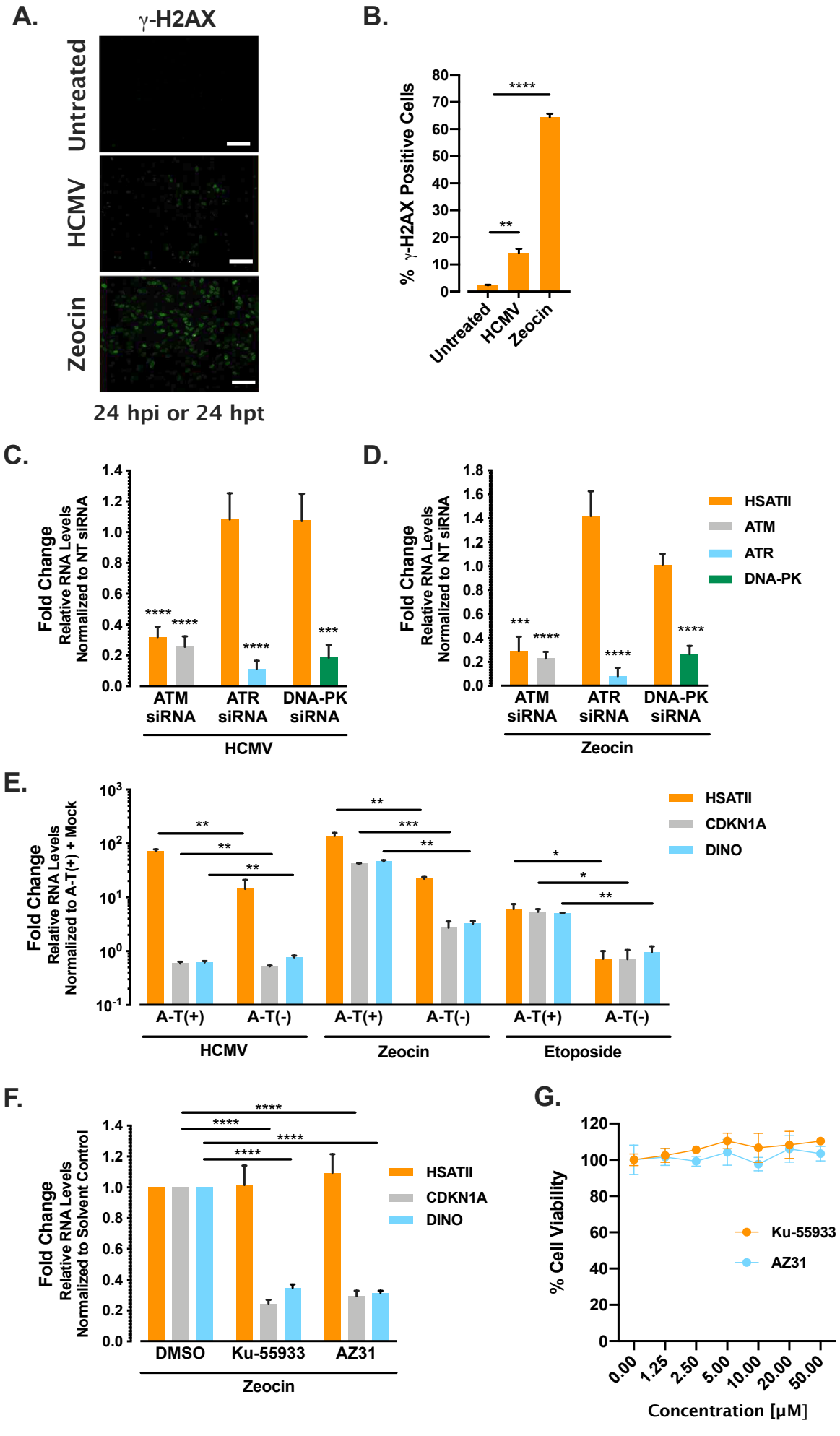
A.
γ-H2AX
Untreated
HCMV
Zeocin
24 hpi or 24 hpt
B.
% γ-H2AX Positive Cells
Untreated
HCMV
Zeocin
C.
Fold Change
Relative RNA Levels
Normalized to NT siRNA
ATM siRNA
ATR siRNA
DNA-PK siRNA
HCMV
D.
Zeocin
HSATII
ATM
ATR
DNA-PK
E.
Fold Change
Relative RNA Levels
Normalized to A-T(+) + Mock
HSATII
CDKN1A
DINO
A-T(+)
A-T(-)
HCMV
Zeocin
Etoposide
F.
Fold Change
Relative RNA Levels
Normalized to Solvent Control
DMSO
Ku-55933
AZ31
G.
% Cell Viability
Ku-55933
AZ31
Concentration [μM]

Figure 6.

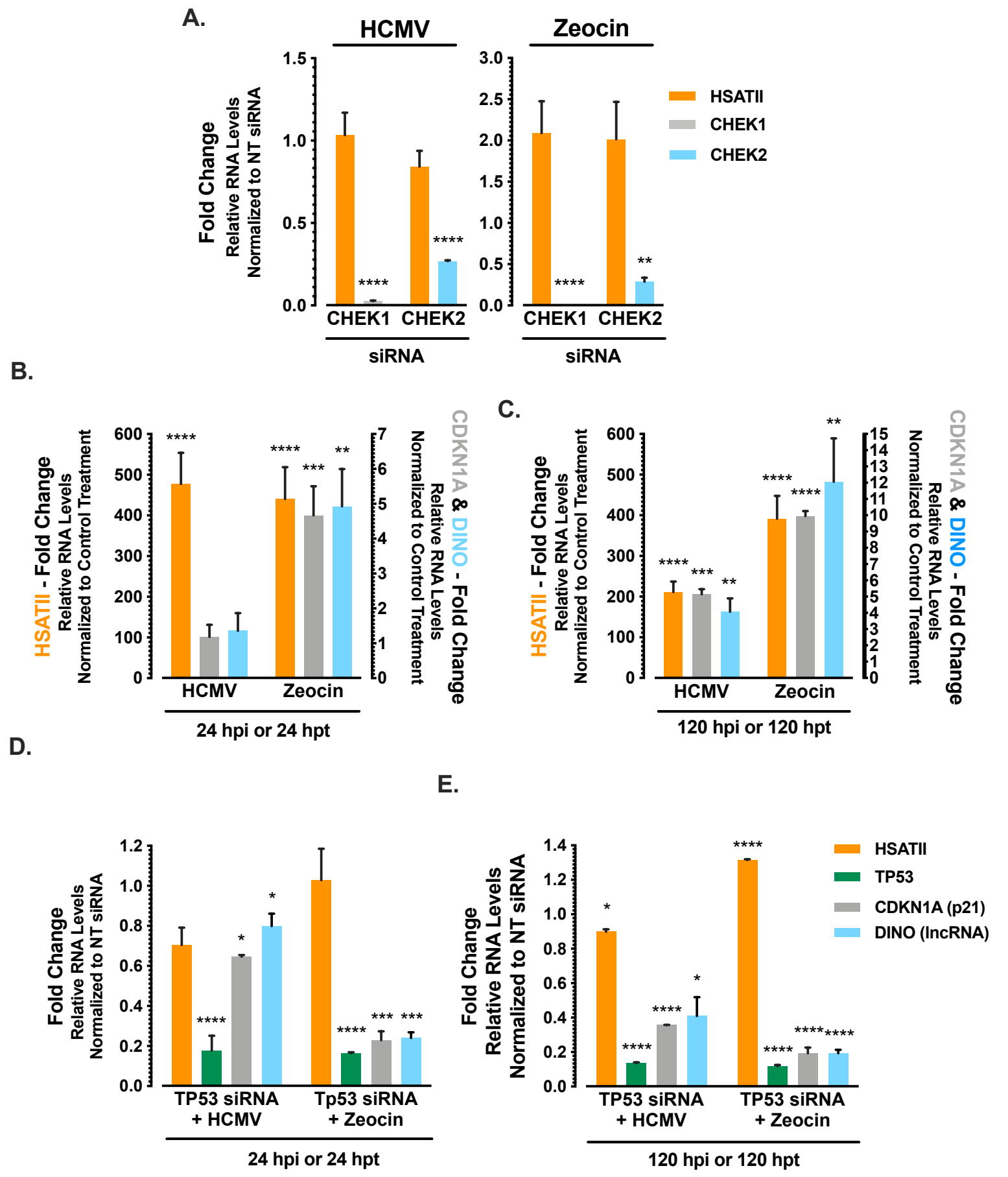
A.
HCMV
Zeocin
Fold Change
Relative RNA Levels
Normalized to NT siRNA
HSATII
CHEK1
CHEK2
CHEK1 CHEK2
siRNA
B.
HSATII - Fold Change
Relative RNA Levels
Normalized to Control Treatment
CDKN1A & DINO - Fold Change
Relative RNA Levels
Normalized to Control Treatment
HCMV
Zeocin
24 hpi or 24 hpt
C.
120 hpi or 120 hpt
D.
TP53 siRNA + HCMV
Tp53 siRNA + Zeocin
24 hpi or 24 hpt
E.
TP53
CDKN1A (p21)
DINO (lncRNA)
TP53 siRNA + HCMV
TP53 siRNA + Zeocin
120 hpi or 120 hpt

Figure 7.

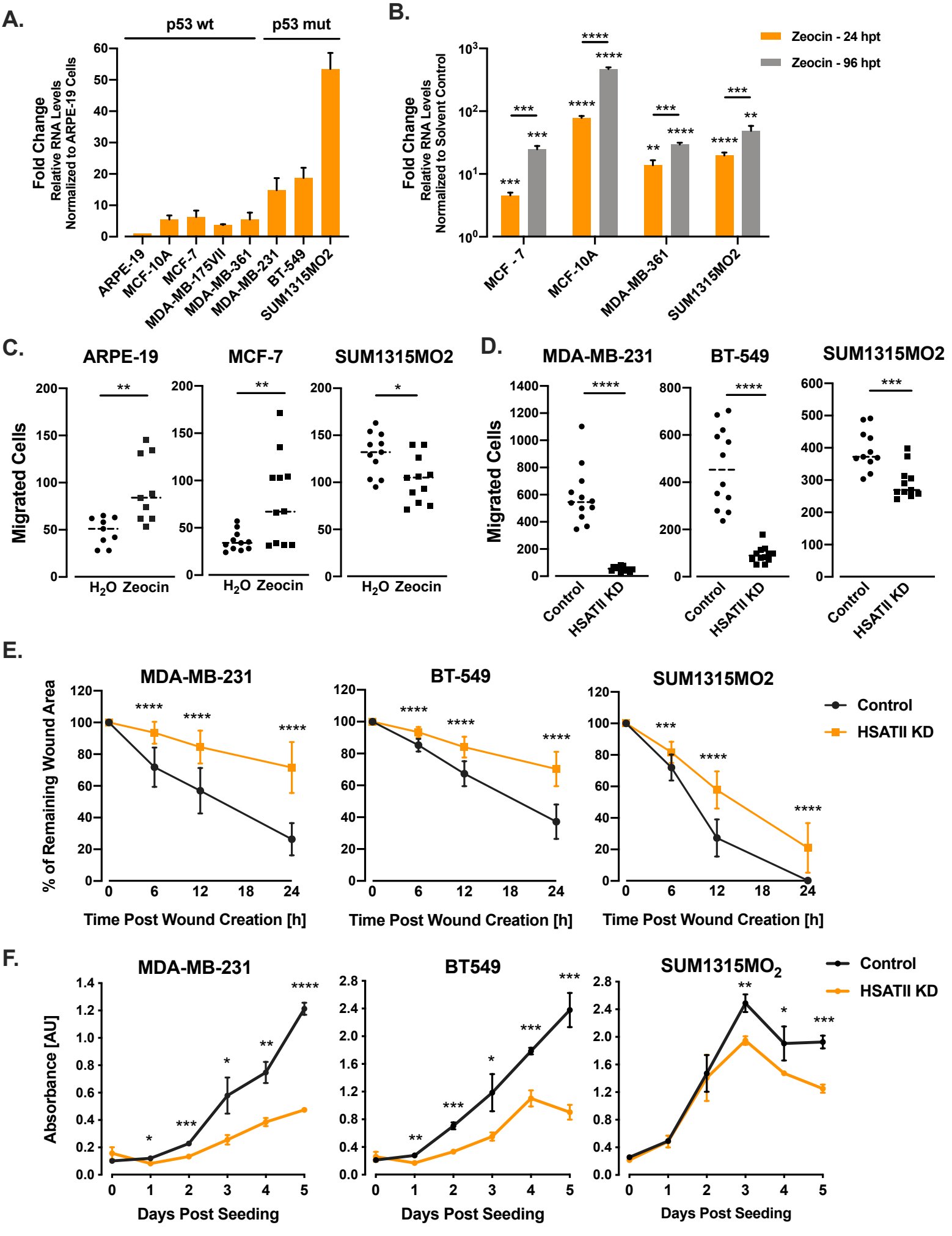
A.
p53 wt
p53 mut
Fold Change
Relative RNA Levels
Normalized to ARPE-19 Cells
ARPE-19
MCF-10A
MCF-7
MDA-MB-175VII
MDA-MB-361
MDA-MB-231
BT-549
SUM1315MO2
B.
Zeocin - 24 hpt
Zeocin - 96 hpt
Fold Change
Relative RNA Levels
Normalized to Solvent Control
MCF - 7
MCF-10A
MDA-MB-361
SUM1315MO2
C.
ARPE-19
MCF-7
SUM1315MO2
Migrated Cells
H2O Zeocin
D.
MDA-MB-231
BT-549
SUM1315MO2
Migrated Cells
Control
HSATII KD
E.
MDA-MB-231
BT-549
SUM1315MO2
% of Remaining Wound Area
Control
HSATII KD
Time Post Wound Creation [h]
F.
MDA-MB-231
BT549
SUM1315MO2
Absorbance [AU]
Control
HSATII KD
Days Post Seeding